IMPACT OF A LAKE BREEZE ON SUMMER OZONE CONCENTRATION IN THE SALT LAKE VALLEY

by

Brian Kenneth Blaylock

A thesis submitted to the faculty of
The University of Utah
in partial fulfillment of the requirements for the degree of

Master of Science

Department of Atmospheric Sciences

The University of Utah

December 2016

The University of Utah Graduate School

STATEMENT OF THESIS APPROVAL

The thesis of **Brian Kenneth Blaylock**

has been approved by the following supervisory committee members:

John D. Horel	, Chair	**July 13, 2016** Date Approved
Erik Travis Crosman	, Member	**July 13, 2016** Date Approved
John Chun-Han Lin	, Member	**July 13, 2016** Date Approved

and by **Kevin Perry** , Chair/Dean of

the Department/College/School of **Atmospheric Sciences**

and by David B. Kieda, Dean of The Graduate School.

ABSTRACT

During the late afternoon of 18 June 2015, ozone concentrations within a strong lake breeze arising from the Great Salt Lake in northern Utah were observed to be ~20 ppb higher than those in its advance. Ozone observations from an enhanced network were available from state air quality measurement sites, additional fixed locations, and mobile platforms, including a news helicopter. The southward progression of the well-defined lake-breeze front through the Salt Lake Valley was observed by wind, temperature, and moisture observations available at automated weather stations, as well as radial velocity scans from a nearby Terminal Doppler Weather Radar. Strong flow opposing the lake breeze increased convergent frontogenesis and delayed the onset of its passage through the Salt Lake Valley. Ozone concentrations were exceptionally high aloft in the head of the lake-breeze front.

The development and progression of lake breezes on both 17 and 18 June 2015 were simulated using the Weather Research and Forecast model at 1-km horizontal resolution over northern Utah. The model was initialized at 0000 UTC 14 June 2015 using hourly analyses at 3-km resolution from the High Resolution Rapid Refresh model. The underlying surface state was improved by specifying the areal extent and surface temperature of the lake observed during June 2015. An urban canopy parameterization was added as well to better simulate urban effects on wind and heat fluxes. These modifications improved the model simulation particularly for the more typical lake

breeze event on 17 June. However, on 18 June weaker than observed opposing southerly flow allowed the development of the simulated lake-breeze front to occur too early and its subsequent speed up the valley was too fast. Continuous passive tracers initialized at the surface within and ahead of the lake breeze highlight the dispersion and transport of pollutants arising from the strong lake-breeze front on 18 June. Tracers within the lake breeze are confined closer to the surface while tracers in advance of the front are lofted vertically over it.


GSLSO
2015

TABLE OF CONTENTS

LIST OF TABLES

LIST OF FIGURES

ACKNOWLEDGEMENTS

Completing a master's degree is not an easy task, and there are many people who have supported me I wish to recognize. First, this work would not have been possible without the guidance from my advisor, Dr. John Horel. I am grateful for the opportunity to work with the Horel research group on various projects, which has helped me develop the skills needed to complete this master's degree and has prepared me for my Ph.D. research and a future career. My gratitude also goes out to Erik Crosman, whose comments and expertise added much value to this research. Also, I'd like to thank John Lin for serving on my committee and the suggestions offered in preparing this thesis.

This research was supported by a grant from the Utah Division of Air Quality. I appreciate the assistance of Utah's Division of Air Quality and the entire Great Salt Lake Summer Ozone Study team, who made the field work this thesis is based on possible. Computer resources and troubleshooting provided by the Center for High Performance Computing at the University of Utah are also appreciated. My graduate career has especially been enriched by my attendance and participation at various meetings, conferences, and the WRF Tutorial. Thank you Nola Lucke for making the necessary travel arrangements!

Finally, I wish to thank my parents, siblings, friends, and classmates whose love and support make life enjoyable every day.

CHAPTER 1

INTRODUCTION

1.1 Overview of Ozone Pollution and Lake Breezes

Ozone is an invisible gas harmful to people's respiratory health (Sousa et al. 2013). While ozone formed naturally in the stratosphere does not usually pose a threat, tropospheric ozone formed by photochemical reactions of urban or natural pollutants is hazardous. Because ozone formation depends on sunlight, ozone concentrations are typically maximized in the late afternoon during summer months when solar insolation is greatest. Unfortunately, many people across the United States are exposed to unhealthy levels of ozone pollution. Groups with the greatest risk of adverse health effects include children, elderly, individuals with respiratory diseases, and people who work and recreate outdoors.

Because of ozone's impact on public health, in 2015 the Environmental Protection Agency (EPA) tightened the 8-hour National Ambient Air Quality Standard (NAAQS) for ozone from 75 ppb to 70 ppb (EPA 2015). According to ozone observations in 2014, 241 counties in the United States would have exceeded the updated NAAQS ozone levels (Figure 1.1). Ground-level ozone concentrations frequently exceed this standard in northern Utah. For example, Figure 1.2 shows the maximum 8-hr ozone concentration observed each day at the Utah Division of Air Quality (DAQ) monitoring site at Hawthorne

Elementary in Salt Lake City for the summer months between 2011 and 2015. Several periods that exceed NAAQS were observed each year. Metropolitan as well as rural areas in the western United States may have difficulty complying with the updated standard since background ozone levels—ozone not caused by North America anthropogenic emissions (i.e., Asian pollution and natural sources, including wildfires)—are often high in this region (Jaffe 2011). Thus, implementing effective ozone reduction plans and improving air quality forecasts in these states require a deeper understanding of local factors that exacerbate ozone pollution.

Air quality in the highly urbanized corridor on the east side of the Great Salt Lake (GSL) in northern Utah is largely controlled by its complex geography (Figure 1.3a) and attendant meteorology. The densely populated Salt Lake Valley to the southeast of the GSL is bounded by the Wasatch Mountains to the east and the Oquirrh mountains to the west (Figure 1.3b). The surrounding terrain, variable underlying land surface characteristics, and the GSL contribute to thermally driven flows that influence the development, transport, and destruction of air pollutants within the Valley (Stewart et al. 2002; Ludwig et al. 2004). For example, afternoon lake breezes penetrating southward into the Salt Lake Valley are very common on clear summer days and arise from differential heating between the GSL, the valley floor, and surrounding terrain (Zumpfe and Horel 2007). The lake breezes are typically superimposed on the daytime up-valley flow, which provides a continuous daytime up-valley transport mechanism throughout the SLV on synoptically undisturbed days (Crosman and Horel 2010).

Lake breeze and sea breeze circulations have been well documented and studied for many years (Miller et al. 2003), including many numerical modeling studies of such events

(Crosman and Horel 2010). Differential daytime heating between water and land creates a horizontal temperature and pressure gradient with lower temperatures and higher pressure over the body of water and higher temperatures and lower pressure over land. Propagation of the density current is characterized by near-surface winds that advect cooler air from over the water inland, stabilizing the lower boundary layer. Intense vertical motions may be observed at the leading edge or head of the lake or sea breeze front. Frontogenesis at the lake-breeze frontal boundary can be especially strong in the presence of moderate opposing winds due to convergence. The circulation is completed by a return flow aloft and descending motions over the body of water to compensate for the mass flux. These thermally driven wind circulations typically occur on clear days when solar radiation is maximized and when there is little synoptic disturbance. In the Salt Lake Valley, with the lake positioned to the north of the city, a lake breeze will reverse winds from southerly to northerly as the lake front passes (Zumpfe and Horel 2007).

The impact of ocean coastal regions and lakes on urban air quality has been extensively studied in many regions of the world. The thermally driven coastal or lake-shore circulations impact pollutant transport through a number of processes, including vertical mixing, horizontal advection, and recirculation, while the water surfaces impact the pollutant chemistry by providing both a reservoir for precursor pollutants and an environment with lower rates of ozone deposition and nocturnal destruction (Burley et al. 2015). Daytime breezes transport precursor pollutants and a stable marine boundary layer inland, impeding vertical mixing within the urban region concurrent with the daytime sunlight that drives photochemical ozone production, while nighttime land breezes transport pollutants from the urban regions over the adjacent water bodies (Sills et al. 2011;

Wentworth et al. 2015). The impact of thermally driven flows on summer air quality have been studied in many major coastal metropolitan areas, e.g., Los Angeles (Lu and Turco 1995), Milwaukee (Lennartson 2002), Houston (Banta et al. 2005), Chicago (Foley et al. 2011), Maryland (Stauffer et al. 2015), Toronto (Hastie et al. 1999; Wentworth et al. 2015), and southwest Ontario (Levy et al. 2010; Hayden et al. 2011; Sills et al. 2011). This study, however, represents the first detailed study to investigate the impacts of thermally driven flows on ozone transport within the Great Salt Lake basin.

The interactions between the large-scale synoptic environment and thermally driven circulations play an important role in modulating the day-to-day ozone variability in coastal regions. When a 2-8 m s^{-1} synoptic geostrophic wind opposes the daytime sea- or lake-breeze circulation, the effect is typically convergent frontogenesis of the breeze front, which results in 1) a delayed onset of the breeze circulation at the coastline, 2) a much slower rate of inland frontal movement, and 3) enhanced convergence within and behind the frontal zone (Arritt 1989; Arritt 1993; Gilliam et al. 2004; Porson et al. 2007; Crosman and Horel 2010; Ji et al. 2013). Several studies have documented the enhancement of ozone concentrations along convergent frontogenesis of sea- and lake-breeze fronts. Gaza (1998) found elevated ozone and precursors in a narrow zone at and south of a sea breeze coastal boundary in the northeastern US associated with convergence and a strong capping inversion behind the front. Oh et al. (2006) and Hwang et al. (2007) found enhanced ozone concentrations due to convergent frontogenesis and a stalled sea-breeze front during opposing flow in the near-shore regions of several metropolitan areas in Korea. In the Salt Lake Valley, convergent frontogenesis along a lake-breeze front was shown to impact $PM_{2.5}$ concentrations in the Salt Lake Valley by Crosman and Horel

(2016). In this study, we investigate the impact of the convergent frontogenesis on ozone during a particularly strong lake-breeze frontal episode.

High ozone concentrations during summer instigated by sea or lake breezes have been difficult to simulate and forecast, especially in operational numerical air quality models (Lu and Turco 1995; Banta et al. 2005; Angevine et al. 2006; Bao et al. 2008; Crosman and Horel 2010; Angevine et al. 2012). Inaccurate initialization, including incomplete specification of coastline characteristics and water surface temperatures, are some of the factors impeding such numerical forecasts (Crosman and Horel 2012; Lombardo et al. 2016). Improving the surface initialization of the lake characteristics was an important aspect of this study's lake breeze simulation.

The case studies by Zumpfe and Horel (2007) and Crosman and Horel (2016) illustrate how GSL breezes occurring during all seasons can vary in terms of onset time, propagation speed, and frontal intensity. This thesis focuses on lake breezes affecting ozone pollutant concentrations on 17-18 June 2015. We view the lake breeze on 17 June as a canonical case with features common to many others examined over the years. We will draw greater attention to the lake breeze on 18 June due to its later onset and stronger intensity, resulting from enhanced convergent frontogenesis of the lake breeze. In addition, the role of the lake breezes on ozone concentrations reverse between the two days: the lake serves as a reservoir of cleaner air on 17 June and more polluted air on 18 June.

This thesis will explore the physical processes that influenced ozone concentrations within lake breezes on 17 and 18 June 2015. The atmospheric conditions preceding and during the lake breeze event are evaluated with observations made available by the Great Salt Lake Summer Ozone Study, a field study during the summer of 2015 discussed in

further detail in section 1.2. Those observations are validated and compared with a high-resolution numerical model explained in section 2.2. Passive tracers within the simulation are used to illustrate the three-dimensional transport of pollutants by lake breezes on those days. This study shows how a mesoscale feature affected the development of a strong lake breeze in the Salt Lake Valley and how that lake breeze event impacted air quality, particularly ozone concentration. These findings will be of particular interest to air quality forecasters in coastal environments as well as researchers who use numerical simulations to understand transport of atmospheric pollutants.

1.2 The 2015 Great Salt Lake Summer Ozone Study

As described by Horel et al. (2016), DAQ initiated the Great Salt Lake Summer Ozone Study ($GSLSO_3S$) in 2015 to develop a more complete understanding of the GSL's influence on summer ozone. This study was a collaboration between DAQ and researchers at the University of Utah, Utah State University, and Weber State University. In Utah, summer ozone pollution seems to be less concerning to residents than winter particulates, which is a much more visible pollutant that often plagues the valleys during winter time inversions. This field study drew attention from the media and sparked some community awareness of the summer pollution in the Salt Lake Valley. The primary goals of $GSLSO_3S$ were to 1) determine the areal and vertical extent of summer ozone over and surrounding the GSL and 2) improve understanding of the physical processes that control summer ozone near the GSL to improve air quality forecasts (Horel et al. 2016).

In order to collect adequate data with the limited funds available, the participating researchers leveraged existing infrastructure and took advantage of real-time data

collection to maximize use of the available resources. Routine air quality and meteorological observations in the valley were supplemented by additional observation sites and special platforms deployed for the duration of the June through August study period. The routine observations include permanent DAQ air quality monitoring sites, rawinsondes launched by the National Weather Service twice a day at the Salt Lake International Airport, lake temperature observations at a buoy in the GSL, a Terminal Doppler Weather Radar, and surface meteorological instruments available through the MesoWest cooperative network. Supplementary observations deployed for the study included additional ozone sensors especially concentrated at locations near the GSL, two sodars, a lidar, two laser ceilometers, tethered sonde, as well as mobile ozone observations on board a Utah Transit Authority TRAX train, KSL-TV News helicopter, unmanned aerial vehicle, and road vehicles, including the University of Utah Nerdmobile. Road vehicles typically drove around the perimeter of the lake and partway across the Union Pacific Railroad causeway that bisects the GSL. The TRAX train drove on routes in the Salt Lake Valley referred to as the Red, Green, or Blue lines. The KSL-TV News helicopter flew at various times of day and altitudes as the pilot flew around the valley for routine traffic coverage or news stories. Overall, 88% of the study period days had at least one form of mobile ozone measurements to complement the daily observations at the fixed ozone monitoring sites. An archive of the data collected during the study is available online at http://meso2.chpc.utah.edu/gslso3s/.

Three intensive observation periods were conducted during the summer—one week during each month. Since many of the available ozone levels and meteorological conditions could be monitored in real-time, mobile observation platforms could be deployed on short

notice and target observations at the most interesting parts of the valley. This ability to rapidly deploy mobile observations when needed made the field study especially successful. The initial study findings revealed that ozone pollution is not uniform across the Salt Lake Valley. The range of ozone concentrations observed across the observing sites was often between 30-60 ppb. During the 2015 summer (months June, July, August), ozone concentrations in excess of NAAQS were observed on 30 days at one or more GSLSO_3S stationary sites in the vicinity of the GSL.

The work presented in the remainder of this thesis addresses the second purpose of the GSLSO_3S by exploring the physical processes that caused elevated ozone concentration within a lake breeze on 18 June 2015. The core research described here has been submitted as a manuscript to the *Journal of Applied Meteorology and Climatology* (Blaylock et al. 2016). The manuscript of this thesis examines the structure and propagation of a lake breeze with the extensive meteorological and ozone observations available in the valley on that day. Then the ability of a high-resolution weather model to simulate the lake breeze event, with improvements made to the initialized surface characteristics, is evaluated. Passive tracers used in the simulation demonstrate how pollutants within the lake breeze and ahead of the lake-breeze front interact at the frontal boundary.

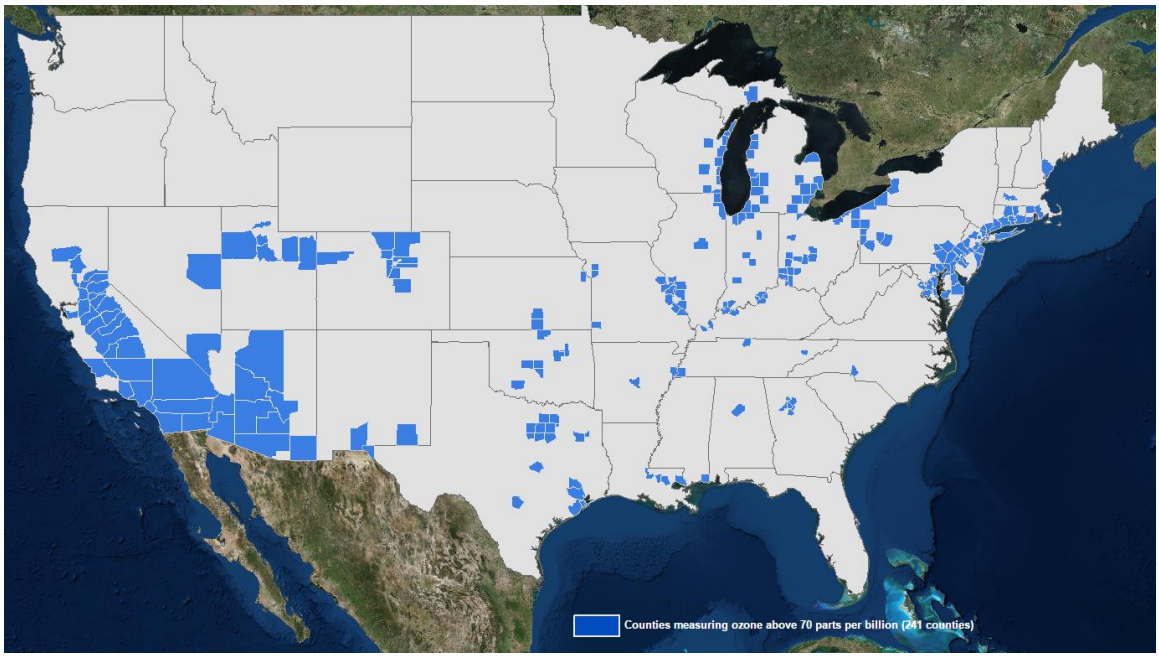

Figure 1.1. Counties that exceed the new ozone NAAQS using data from 2014. Source: EPA [https://ozoneairqualitystandards.epa.gov/OAR_OAQPS/OzoneSliderApp/index.html#]

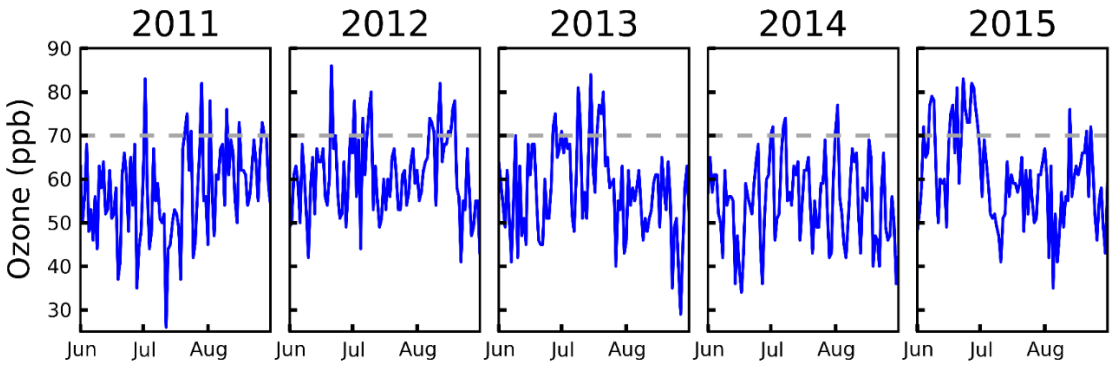

Figure 1.2. Daily maximum 8-hr ozone concentration at DAQ's Hawthorne Elementary site. The NAAQS is marked by the dashed line.

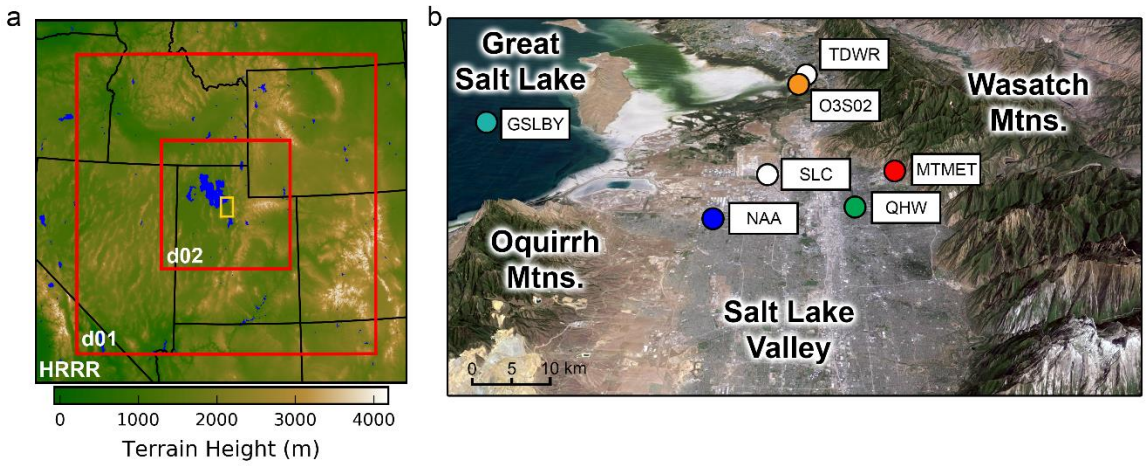

Figure 1.3. Salt Lake Valley study area and simulation domains. (a) HRRR model terrain (shaded according to scale) with nested WRF domains outlined in red and Salt Lake Valley region in yellow. (b) Observation sites discussed in the text: USGS Great Salt Lake buoy (GSLBY), Terminal Doppler Weather Radar (TDWR), Salt Lake International Airport (SLC), Farmington Bay (O3S02), Neil Armstrong Academy (NAA), University of Utah Mountain Meteorology Lab (MTMET), and DAQ Hawthorne Site (QHW).

CHAPTER 2

DATA AND METHODS

2.1 Meteorological and Ozone Observations

As described by Horel et al. (2016), the GSLSO_3S took advantage of existing observational infrastructure and also relied on additional sensors deployed during the summer. Atmospheric conditions in northern Utah were monitored at over 100 in situ automated surface stations available through the MesoWest cooperative network (Horel et al. 2002). Near-surface and upper-air observations near the lake are available from rawinsondes launched at the Salt Lake International Airport (SLC in Figure 1.3b) in the morning (1200 UTC) and evening (0000 UTC). A Terminal Doppler Weather Radar (TDWR) located directly north of the Salt Lake Valley (see Figure 1.3b) measured radial wind velocities in the western half of the Salt Lake Valley (beam blockage by intervening terrain restricts observation in the east half of the valley). A buoy in the south arm of the GSL (GSLBY) deployed by the United States Geological Survey (USGS) measured meteorological parameters as well as water temperature at fourteen levels in the vertical. Ozone concentrations in northern Utah were measured at eight permanent DAQ sites as well as from 16 temporary sensors deployed by DAQ and the University of Utah in the vicinity of the lake. We focus here on four sites with ozone monitors co-located with meteorological sensors in the valley—O3S02, NAA, QHW, and MTMET (Figure 1.3b).

The sampling interval at O3S02, NAA, and MTMET was 5 min, whereas QHW had a sampling interval of 15 min.

Additional ozone sensors were mounted on several vehicles as well as two unique platforms during GSLSO$_3$S: (1) a public-transit light rail car, known as TRAX, operating on electrified routes, and (2) the KSL-TV news helicopter. The reporting intervals for these ozone observations were 1 min and 10 s, respectively. Many of the helicopter's summer flight times and flight paths were determined by the pilot's routine traffic reports and other news reporting needs. We requested the pilot make an overflight of the GSL during the afternoon of 17 June 2015 with vertical profiles from close to the surface to 1000 m AGL. Fortuitously, during the afternoon of 18 June 2015, the pilot flew the helicopter down the center of the valley through the lake-breeze front at elevations between 1400 and 1700 m MSL (100-400 m AGL).

2.2 WRF Model Simulation

2.2.1 WRF Configuration

A high-resolution simulation of the atmospheric conditions for the lake breeze events on 17-18 June 2015 was completed using the Weather Research and Forecast (WRF) model version 3.7 with Advanced Research WRF dynamical core (see Table 2.1 for a summary of the configuration details). Initial and boundary conditions were retrieved from the National Centers for Environmental Prediction High Resolution Rapid Refresh (HRRR) model hourly analyses beginning at 0000 UTC 14 June 2015 and continuing until 0700 UTC 19 June 2015 (Benjamin et al. 2016). Two WRF domains with one-way nesting within the 3-km horizontal resolution HRRR domain were used as shown in Figure 1.3a.

The outer 3-km domain, d01, covers all of Utah and parts of the surrounding states while the inner 1-km domain, d02, is focused on northern Utah. Both domains are centered over Salt Lake City, with 30 vertical eta levels between the surface and 50 hPa. The MODIS 30-arc-second land use classification—also used by the HRRR model—is used in this simulation except for the modifications discussed in section 2.2.2.

This numerical simulation work is unique from others because we have initialized our simulation with the HRRR boundary conditions. In other similar studies, atmospheric models, such as the North America Mesoscale (NAM) model or North American Regional Reanalysis (NARR), are most frequently used to initialize WRF simulations. This effort is the first one, to our knowledge, to use this state-of-the-art data assimilation system as a means to initialize the WRF for research simulations of an air pollution episode. While the main purpose of the HRRR is to aid severe storm forecasters and air traffic managers, there are advantages of using HRRR analyses in air quality studies. The HRRR uses the popular WRF-ARW (the same dynamical core used in this research), has advanced data assimilation capabilities, and produces hourly analyses at 3-km horizontal resolution, making it the highest resolution operational model over the continental United States. With this high temporal and horizontal resolution model driving WRF boundary conditions we assume the resulting WRF simulated lake breeze and terrain flow is superior over a simulation that would have used NAM or NARR boundary conditions or otherwise using raw operational weather model output. Although we use high temporal and spatial resolution boundary conditions, there are still notable errors introduced by the HRRR analysis that affect the lake breeze simulation. Consequently, modifications are made to address the HRRR's shortcomings, and are discussed in section 2.2.2.

2.2.2 WRF Modifications

Lombardo et al. (2016) discuss the sensitivity of simulated sea breezes in Connecticut and New York to inaccurate coastlines and sea surface temperature when initializing simulations from coarse 32-km NARR grids. These types of errors are even prevalent in the fine-grid 3-km HRRR. Inspection of the land use categories within the HRRR model revealed obvious errors in the areal extent of the GSL, arising from the reliance on a 2001 MODIS image when the lake level was much higher than in 2015 (Figure 2.1b). The GSL lies within an endorheic basin whose level has been strongly affected by drought and increased water use (Wurtsbaugh et al. 2016). During the 2015 summer, the GSL was near record low levels, as evident in the MODIS image on 18 June 2015 (Figure 2.1a). The specified lake temperature in the HRRR analyses was also much too low (Table 2.2). Hence, it is not surprising that using the MODIS land use categories and lake surface temperature specified by the HRRR in initial test simulations led to erroneously low boundary layer depths over the lake, strong lake-land temperature contrasts, and overly strong lake breezes (not shown).

To overcome the deficiencies in the areal extent and lake temperature available from the HRRR, Figure 2.1c illustrates the modifications applied for the WRF simulations of this study. Model grid points that are no longer lake were reclassified as “barren or sparsely vegetated” land to represent the exposed, dry lake bed (compare Figures 2.1b and 2.1c). In addition to the average HRRR lake temperature being too cold (Table 2.2), the lowest temperatures are also skewed towards the southwest of the lake’s boundary and the lake edge temperatures are affected by land temperature contamination (Figure 2.1b inset). Based on lake temperature climatology (Crosman and Horel 2009), available estimates of

lake surface temperature from an AVHRR thermal image at 2330 UTC 18 June 2015 and subsurface temperature from the GSLBY buoy on that day, the temperature of the GSL was modified to a uniform temperature of 28.9 °C (Figure 2.1c inset) to represent the afternoon lake surface temperature. Although the lake surface temperature remains fixed throughout the simulation (a limitation of the WRF model), the land surface temperatures evolve on the basis of the Noah land surface model parameterization.

The treatment of urban effects in the Salt Lake Valley was also improved by enabling the urban canopy model for the WRF model, which is not used in the HRRR. Parameters in that scheme were modified to better represent the Salt Lake Valley. For example, the Salt Lake Valley during summer contains many regions that resemble an urban forest with dense vegetation and large swaths of irrigated lawns. Thus, the percentage of vegetation in the urban land use category was increased from the default setting of 10% to 50% to help reduce near-surface wind speeds and cool the urban area. Small increases to the average building height and road width were also made from the default settings to conform more closely to the local environment.

These modifications did not attempt to repair all errors introduced by the HRRR analysis, but resulted in a better simulation of the lake breeze than simply running WRF with HRRR boundary conditions and default settings. Sensitivity studies of each of these modifications are not presented in this thesis. Instead, the simulated lake breeze is evaluated and used to show how pollutants within the lake breeze and in the ambient air are influenced by the lake-breeze front. Although it is later shown that the simulated lake breeze has discrepancies in its time of onset and speed down the Salt Lake Valley, the

simulation is used to examine some of the characteristics of the lake breeze in ways not possible from the available observations.

Table 2.1: HRRR and WRF model configuration.

Setting or Option	HRRR	d01 (d02)
WRF Version	WRF 3.6	WRF 3.7
Boundary Conditions	Rapid Refresh (RAP)	HRRR (d01)
Land Surface	30 arch-sec MODIS 21 category	30 arch-sec MODIS 21 category
dx/dy	3 km	3 km (1 km)
Vertical Levels	50	30
Model Top	20 hPa	50 hPa
Time Step	20-sec	6-sec (2-sec)
Microphysics	Thompson	Thompson
Radiation	RRTMG	RRTMG
Planetary Boundary Layer	MYNN	Mellor-Yamada-Janjic
Surface Layer	RUC land surface model	Unified Noah land-surface model
Cumulus Scheme	No cumulus parameterization	No cumulus parameterization

Table 2.2: Estimates of Great Salt Lake temperature for 18 June 2015.

Lake Temperature (°C)	
Afternoon buoy water temperature at 0.4 meters below surface	27.3
AVHRR satellite (2330 UTC, 5:30 PM local)	27-30
HRRR lake area average.	22.5
WRF modified See Fig. 2.1c	28.9

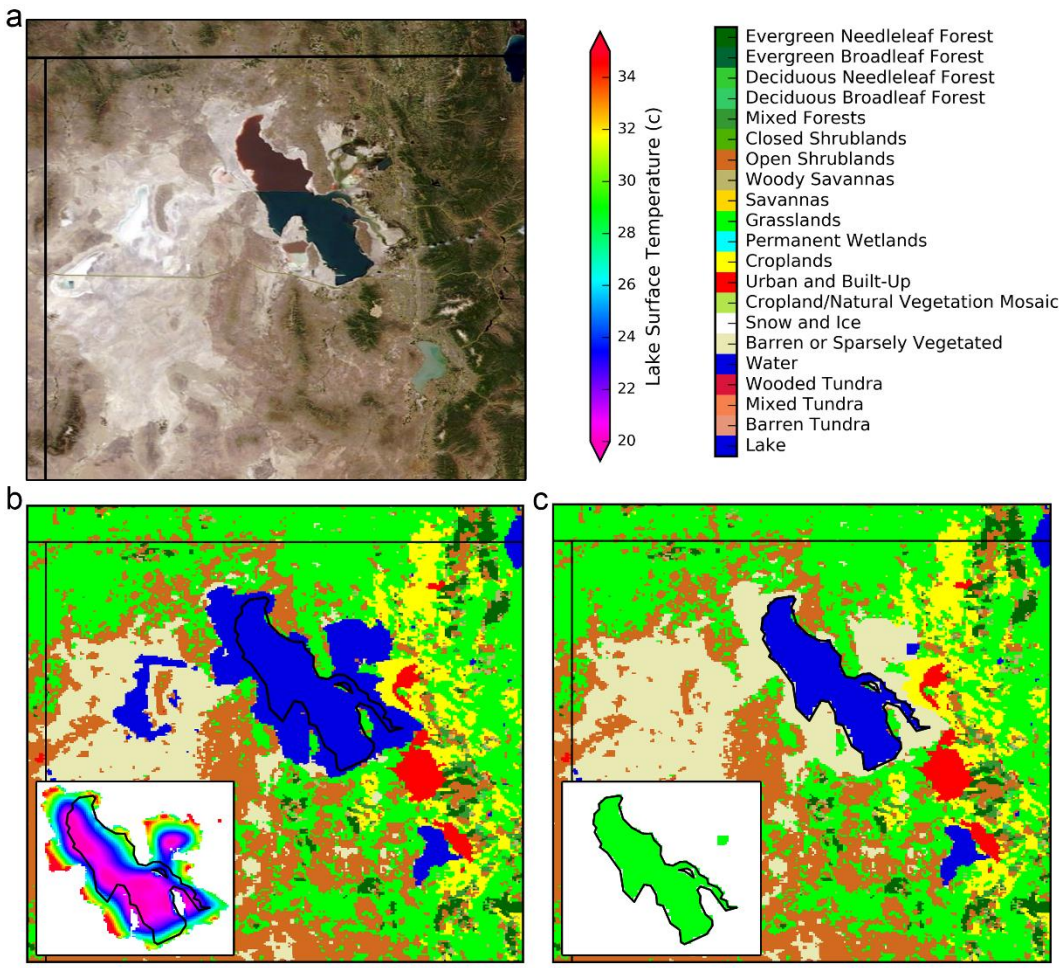

Figure 2.1. Satellite image of northern Utah compared with WRF land use categories. (a) MODIS true color satellite image on 18 June 2015. (b) MODIS 30-arc-second land use categories (defined by the color bar in the upper right) used in HRRR and WRF models with Great Salt Lake at record high levels and a pool of water in the west desert. Black outline delineates the lake extent during summer 2015. Inset: Great Salt Lake size and lake surface temperature (according to color bar in upper right) initialized by HRRR analyses. (c) As in (b) except lake size adjusted to 2015 level. Inset: modified lake size with uniform lake surface temperature (28.9 °C).

CHAPTER 3

RESULTS AND DISCUSSION

3.1 Observations of 17-18 June 2015 Lake Breeze Events

The synoptic weather pattern during the week encompassing 17-18 June 2015 was dominated by a longwave ridge over the western United States. These conditions led to low cloud amounts and strong solar insolation—an optimal environment for both a strong lake breeze and photochemical production of ozone. On 17 June, the background synoptic flow remained weak and the lake breeze system developed largely uninfluenced by the synoptic flow. These situations are often referred to as 'classic' lake-breeze cases in the literature (Crosman and Horel 2010). On 18 June, however, channeled synoptic flow resulted in an enhanced southerly flow into the Salt Lake Valley, resulting in the ideal conditions for convergent frontogenesis of the lake-breeze front. On the six days prior to 17 June, none of the 18 ozone observation locations in the vicinity of the GSL or nearby urban areas observed 8-h averaged ozone concentrations in excess of 70 ppb, while on 17 and 18 June, NAAQS exceedances were observed at 7 and 12 sites, respectively. On the following day, 19 June, no stations exceeded the threshold.

Potential temperature, mixing ratio, and wind profiles below 3800 m ASL at SLC are shown for the morning and evening of 18 June in Figure 3.1. In the morning sounding, a radiational inversion below 2000 m ASL is evident, with southeasterly winds caused by

the down-valley land breeze towards the GSL (Figure 3.1a). Focusing on the observations above 1500 m ASL since the surface values at the SLC airport are likely not representative of the larger valley environment, the neutral lapse rate in the evening sounding reflects strong mixing leading to nearly constant mixing ratio (Figure 3.1b). Northwest winds below 2000 m ASL and the slightly higher mixing ratio value at ~1600 m ASL are the signatures of the intrusion of the lake breeze past the airport accompanied by opposing winds aloft of 5-10 m s^{-1} from the south-southwest above 3000 m ASL.

The lake breezes progressing through the Salt Lake Valley during the afternoons of 17-18 June were observed continuously by the TDWR as well as in situ weather stations. These observations highlight the differences in the lake breeze propagation between the two days. Snapshots of their progression are provided in Figure 3.2. Down-valley winds towards the GSL dominate the western two thirds of the Salt Lake Valley during both mornings, as evident in Figures 3.2a and 3.2d (1800 UTC is an hour before solar noon). The southerly down-valley flow on 18 June is enhanced by channeled synoptic flow through the gaps of the Traverse Range (Lareau and Horel 2015) and is substantively stronger than that the day before and the flow pushed further north past SLC (white circle). Northwesterly winds in the northwest corner of the valley closest to the GSL oppose the down-valley flows during the morning. Common to many lake-breeze events (Crosman and Horel 2016), the lake-breeze boundary on 17 June traversed southward through much of the valley by 2100 UTC, with distinct pulses during that afternoon (i.e., in-bound/outbound radial velocity couplets are evident in the western half of the valley). By 0000 UTC 18 June (Figure 3.2c), the lake breeze has transited through the entire valley. On the following day, however, the boundary between the down-valley and lake-breeze

flows and associated convergent frontogenesis remained quasistationary due to the stronger southerly winds until after 2000 UTC on 18 June, while temperature, moisture, and ozone concentration discontinuities began to strengthen across it. By 2100 UTC 18 June, the wind shift boundary began to move southward in the center of the valley, passing over SLC and exhibiting the characteristics of a well-defined lake-breeze front (Figure 3.2e). The front progressed down the valley at a relatively slow phase speed of 4-6 km h^{-1} (Figure 3.2f) until reaching the southern terminus of the valley by 0200 UTC 19 June (not shown). During both evenings, the lake breezes rapidly collapsed and southerly winds returned to the valley surface.

The time series in Figure 3.3 of observed temperature, vector wind, and ozone concentrations highlights similarities and differences between the lake breezes during these two afternoons. Consider first the underlying driver of the land and lake breezes evident from the differences in air temperature between the buoy (GSLBY) relative to the other sites—higher temperatures over the lake during early morning, and lower temperatures during the afternoon. Temperatures and photochemical production of ozone at O3S02 to the north of the SLC airport increase rapidly during both mornings reaching peak ozone values of 85-90 ppb at solar noon (1900 UTC). The influence of the GSL's main water body to the west is evident by the lake breeze push from that direction at 2100 UTC on 17 June and 2000 UTC on 18 June, leading to diminished rates of temperature increase and reduced ozone concentrations. This station, sited on the edge of permanent wetlands, is exposed to transport of precursor pollutants from urban areas to the east and south. The ozone concentrations at O3S02 decrease to below 70 ppb on 17 June and hover around 80 ppb on 18 June with the passages of the lake breezes, i.e., the ozone concentrations arriving

from the direction of the main body of the GSL are lower than the peak value observed at solar noon, with 17 June having ~10 ppb lower ozone concentrations than 18 June. Thus, air advected from the lake appears to have been less polluted on 17 June than on 18 June.

Differences in the transition from down-valley to up-valley flows are evident during the two days at NAA located in the western sector of the valley. Two early pulses of northerly-northwesterly winds are evident at 1700 and 1900 UTC on 17 June followed by the more sustained northwesterly push after 2000 UTC that is coupled with a sharp drop in temperature, both of which indicate the lak- breeze front transiting past NAA (refer as well to Figure 3.2b). Ozone concentrations remain at ~70 ppb throughout the rest of the afternoon. During late morning on 18 June, stronger southerly flow opposed the lake breeze and ozone concentrations of ~60 ppb persisted until 2200 UTC, at which point there is a sharp drop in temperature and sharp increase in ozone levels. Observations from a sodar located 4.5 km to the north of NAA also documented the early (1700 UTC) switch from down-valley to weak westerly-northwesterly winds on 17 June (Figure 3.4a). However, on 18 June between 1700-1900 UTC the down-valley winds below 100 m observed by the sodar persisted and actually increased in speed to 8 m s^{-1} until the abrupt passage of the lake-breeze front by 2030 UTC (Figure 3.4b).

In the eastern urban corridor of the valley (QHW) variable wind directions are observed before 2100 UTC on 17 June, with a steady rise in ozone concentrations, peaking near the same time as the final lake-breeze pulse, followed by a steady decrease in ozone. In contrast, sustained southerly flow during midday on 18 June contributes to nearly constant ozone concentrations until the arrival of the lake-breeze front, when a sharp ~20 ppb increase in ozone is observed, similar to that shown previously at NAA. On the

easternmost fringe of the valley (MTMET), midmorning transitions between 1500 and 1800 UTC from easterly downslope/down-canyon flows to upslope westerly flows lead on both days to sharp increases in ozone concentrations, presumably as a result of the local westerly transport of precursor pollutants from the nearby urban regions. As the lake-breeze front, transits NAA, QHW, and MTMET ozone concentrations, increased 15-20 ppb and remain elevated for several hours, similar to a phenomenon observed in the Greater Toronto Area by Wentworth et al. (2015). The seemingly reduced ozone at O32S02 after the lake-breeze passage was similar to the elevated ozone concentrations at the three valley stations. After 0000 UTC 19 June, ozone titration begins to dominate at O3S02, NAA and QHW while concentrations remain elevated (>60 ppb) at MTMET, which is exposed in the evening to air transported from the nearby mountains rather than from within the urban environment.

The KSL helicopter transect from 2050-2200 UTC 17 June was the most extensive flight over the GSL during the summer (Figure 3.5a). The helicopter transited clockwise, originating from near O3S02, and completed two spiral profiles over the GSL, the southernmost spiral over GSLBY. Ozone concentrations over the GSL at the predominant flight level of ~1550 m ASL (250 m AGL) ranged between 50-60 ppb. When the helicopter descended lower than 1350 m ASL (50 m AGL), ozone concentrations increased to 60 ppb in the first spiral and 70 ppb in the second spiral and then dropped below 50 ppb when ascending to 2300 m ASL (1000 m AGL). Hence, higher ozone concentrations over the lake were trapped in a thin layer over the GSL that afternoon. Elevated ozone concentrations at this time were present in the urban area of the Salt Lake Valley east of the GSL, as evident during the beginning and end of the helicopter flight as well as ozone

observations between 65-87 ppb at the fixed sites and the light rail TRAX train (Figure 3.5a).

The afternoon KSL helicopter transect on 18 June was a more typical flight during the summer, transiting from south to north through the Salt Lake Valley from 2240-2340 UTC 18 June (Figure 3.5b). While flying at elevations of 1400-1700 m ASL (150-350 m AGL) in the south end of the valley, the helicopter measured ozone concentrations near 60 ppb, which is consistent with values observed at the surface prior to the frontal passage at NAA, QHW, and MTMET (Figure 3.3c,d,e). When the helicopter crossed the frontal boundary at 2313 UTC, ozone concentrations spiked to 115 ppb. As the helicopter traveled farther north, ozone concentrations remained ~80 ppb, consistent with those observed at O3S02 and other fixed sites (Figure 3.5b). The similar ozone concentrations observed at the helicopter altitude and surface sites indicate that the pollutants below 1700 m ASL (300 m AGL) were well mixed vertically. However, the exceptional ozone concentration observed by the helicopter at the lake-breeze front is a unique observation. The ozone spike aloft at the frontal boundary is likely a result of convergence and lack of titration within the lake-breeze head. The enhanced pollutant concentrations within the head of the lake-breeze front are somewhat evident by elevated TDWR reflectivity at this time (not shown) as suggested by prior observations of the leading edge of lake-breeze fronts (Zumpfe and Horel 2007; Crosman and Horel, 2016), as well as previous studies of strong lake-breeze fronts during convergent frontogenesis in other regions (e.g., Gaza 1998; Hwang et al. 2007).

3.2 WRF Model Simulation

We briefly illustrate using the HRRR model how inaccurate specification of the areal extent and temperature of the GSL affects model analyses and forecasts. Figures 3.1a and 3.1b show the HRRR 1-h forecasts and analyses of vertical profiles of temperature, moisture, and wind valid at 1200 UTC18 June and 0000 UTC 19 June, respectively, at SLC. The largest deviations in the 1-h forecasts relative to those observed are evident in the afternoon, with lower temperatures and excessive low-level moisture forecasted in the boundary layer. This problem is exacerbated at longer lead times, e.g., the HRRR 12-h forecast of surface potential temperature valid at this time is less than 312 K, leading to a cooler lake boundary layer than that observed (not shown). As should be expected, the vertical profiles from the HRRR analyses are constrained strongly by the observed sounding available at this location, leading, for example, to analyzed boundary layer winds at 0000 UTC from the north as an adjustment of the northeasterly 1-h forecast winds to the observed northwesterly winds.

We now return to Figure 3.3 and contrast the model's evolution of wind and temperature at selected locations relative to those observed. While the simulated temperature at GSLBY is higher than that observed during both days (Figure 3.3a), comparisons at other sites over the main body of the GSL suggest that the simulated lake boundary layer over the GSL remains too cool and shallow even after raising the surface lake temperature and allowing several days of model spin-up for the boundary layer over the lake to adjust to that modified temperature. The penetration at GSLBY of the southerly flow associated with the land breezes is evident in both the observations and simulation during the early morning hours of both days, followed by flow reversal to northerly or

northwesterly.

To the north of the SLC airport at O3S02 during both afternoons, the model tends to be too cold and develops northerly flow during mid-day that misses the subtle westerly wind shifts that may have led to the noticeable changes in ozone concentrations at this location (Figure 3.3b). For example, the simulated lake breeze pushes cooler air from the northwest across O3S02 by 1700 UTC on 18 June, three hours before it was observed to penetrate in the westerly burst mentioned previously (Figures 3.2e and 3.2b).

In the northwestern sector of the valley at NAA (Figure 3.3c), the simulated southeasterly-southerly-oriented land breezes during both mornings at the surface are weaker and followed by strong sustained northerly flows after 1700 UTC on 17 June and 1900 UTC on 18 June. Sharp, sustained temperature declines after the passage of the lake-breeze front in the simulation illustrates the stronger than observed intensity of the lake-breeze air mass. The termination of the lake breeze at NAA is also more distinct earlier, with a sharp temperature increase at 0100 UTC (7 PM MDT) both evenings.

The earlier timing and stronger intensity of the simulated lake-breeze frontal passage on 17 and 18 June are also apparent at QHW and MTMET (Figures 3.3d and 3.3e). The sudden burst of southerly flow after 1700 UTC June 18 is captured in the simulation but was shorter in duration than that observed. Hence, the lack of strong opposing flow in the simulation led to an earlier onset of the lake breeze down the valley.

Thus, even after our adjustments to the areal extent and temperature of the GSL and urban canopy, our simulation has a stronger lake breeze at the surface that started down the Salt Lake Valley earlier than observed, particularly on 18 June. However, the simulation provides a wealth of information on the evolution and structure of the lake breezes, as will

be shown hereafter. We focus in the remainder of this section on the 18 June lake breeze that was observed to have higher ozone concentrations within it and lower concentrations in advance of it.

Figure 3.6 delineates the progression of the observed, analyzed, and simulated surface lake-breeze front in the Salt Lake Valley between 1800 and 2300 UTC (local 12:00 to 5:00 PM). Only simulated fields below 1500 m are shown to emphasize the conditions within the lower parts of the valley. We review first the observed progression of the lake-breeze front (dashed lines in center and right panels, see also Figure 3.2). The leading edge of the lake breeze remains quasistationary from 1800 to 2000 UTC as a result of the aforementioned strong southerly opposing flow (Figures 3.6a-c). Then the southerly flow wanes particularly in the central section of the valley and the front advances (Figure 3.6d) and subsequently continues down the valley (Figures 3.6d-e), reaching the southern extent at approximately 0220 UTC that evening (not shown).

Notice how the HRRR analyses handle the lake breeze shown in the left panels in Figure 3.6. The HRRR positions the front at 1800 UTC in the eastern half of the valley ~12 km farther south than was observed. During the rest of the afternoon the HRRR lake-breeze front remains quasistationary near the northern extent of the valley, with little change in its frontal position and orientation. The magnitude of meridional winds on either side of the frontal zone between 1800-2000 UTC varies from hour to hour, perhaps an effect of differences in which data assets were assimilated by the HRRR. The HRRR analyses incorrectly locate the front at the north end of the valley, with little to no up-valley progression during the afternoon. By the time the observed lake-breeze front reached the southern terminus of the valley, the HRRR analysis shows a weakening front still located

north of the center the valley an hour before the lake breeze circulation collapses (not shown).

The center panels in Figure 3.6 show the near-surface moisture content and 10-m meridional wind as well as vector winds plotted every 3-km. The meridional wind component is a proxy to the TDWR radial velocities in Figure 3.2 such that the simulated front is objectively identified as the locations where the meridional wind component reverses and, hence, convergent frontogenesis is particularly evident. As should be expected, the model's inability to develop a sustained strong flow opposing the lake breeze leads to the front being too far south in the central portion of the valley in the early afternoon (Figures 3.6a-b). Subsequently, after 1900 UTC (Figure 3.6c), the front begins to move down the valley too early and too fast by ~3 km h^{-1}, leading to it reaching the southern terminus of the valley several hours earlier than observed (Figure 3.6f). However, the general features of the front's evolution are captured with low mixing ratio and southerly winds in advance of the front and higher mixing ratio and northerly winds to its rear.

The right panels in Figure 3.6 show vertical velocity and vector winds on the seventh level of the terrain-following model coordinate, ~1000 m AGL. Dashed and solid lines again represent the approximate frontal position at the surface. The near-surface convergent frontogenesis leads to upward motion at the frontal boundary coupled to descending motion in its wake that resembles the vertical motion patterns expected aloft that are often associated with a well-defined lake breeze frontal head (Zumpfe and Horel 2007; Crosman and Horel 2016).

Time-height sections of potential temperature and meridional wind at NAA for the

lake-breeze events on 17 and 18 June are shown in Figures 3.7a and 3.7b, respectively. The strong, shallow stable layers during the early morning hours mix out by 1600 UTC on both days but a warmer, deeper, well-mixed boundary layer through the lowest km is evident on 18 June (Figure 3.7b). The strength of the opposing southerly meridional flow near the surface and convergent frontogenesis are much stronger on 18 June (Figure 3.7b). Hence, there is a very well-defined frontal head on 18 June as it passes over NAA. A frontal head only develops on 17 June when the front reaches the southern terminus of the valley (not shown). Northerly winds on both days continue until near sunset (0200 UTC), after which the lake breeze collapses.

Potential temperature and vertical motion along the 3-km-wide A-B cross-section (Figure 3.8a) are shown for 1800, 1900, and 2000 UTC 18 June in Figures 3.8b-3.8d, respectively. The well-mixed warm boundary layer in the lowest km in advance of the front is rapidly replaced as the front passes by with a cooler and more shallow lake-breeze boundary layer. The strong rising/sinking couplets (0.5-2.5 m s^{-1}) at the leading edge of the lake-breeze front head previously shown in Figure 3.8 are well defined here as well. Passive tracers emitted every time step are used to visualize the dispersion and transport of pollutants in the Salt Lake Valley as they interact with the lake-breeze front. The 5x15-km areas at the north and south end of the Salt Lake Valley within which tracers are released in the lowest three model levels are shown in Figure 3.8a as well. Counts of the number of tracers emitted between 1700-2000 UTC 18 June are shown at 1800-2000 UTC in Figures 3.8b-d along the cross-section defined in Figure 3.8a. The blue tracers emitted at the south end of the valley illustrate how precursor pollutants and ozone in the deep boundary layer ahead of the front may be advected northward and lofted over the lake breeze air. Plan view

maps of the tracer counts (not shown) indicate those tracers are transported aloft northeastward across the Wasatch Mountains, which is consistent with the upper level flows evident in Figure 3.6. Red tracers from the north end of the Salt Lake Valley illustrate dispersion of pollutants within the lake breeze. These tracers are transported laterally up the valley and confined near the surface by the capping stable layer, except for the lofting of tracers within the head of the lake-breeze front, where vertical motions are maximized. Turbulent mixing aloft likely dilutes the tracer concentrations from both source regions as the lake-breeze front travels southward. Although the movement of the simulated lake-breeze front down the valley is too rapid, the behavior of the passive tracers illustrated in Figure 3.8 is generally consistent with the observations both at the surface from the fixed and mobile platforms as well as the ozone concentration spike observed by the helicopter. That is, blue tracers mix within a greater boundary layer are more diluted than red tracers within the lake breeze, which are concentrated in a shallow layer within the lake breeze. Missing in the simulation is the effect of photochemical reactions likely dominating near the surface, leading to more titration at lower elevations, with less titration possibly within the head of the lake breeze.

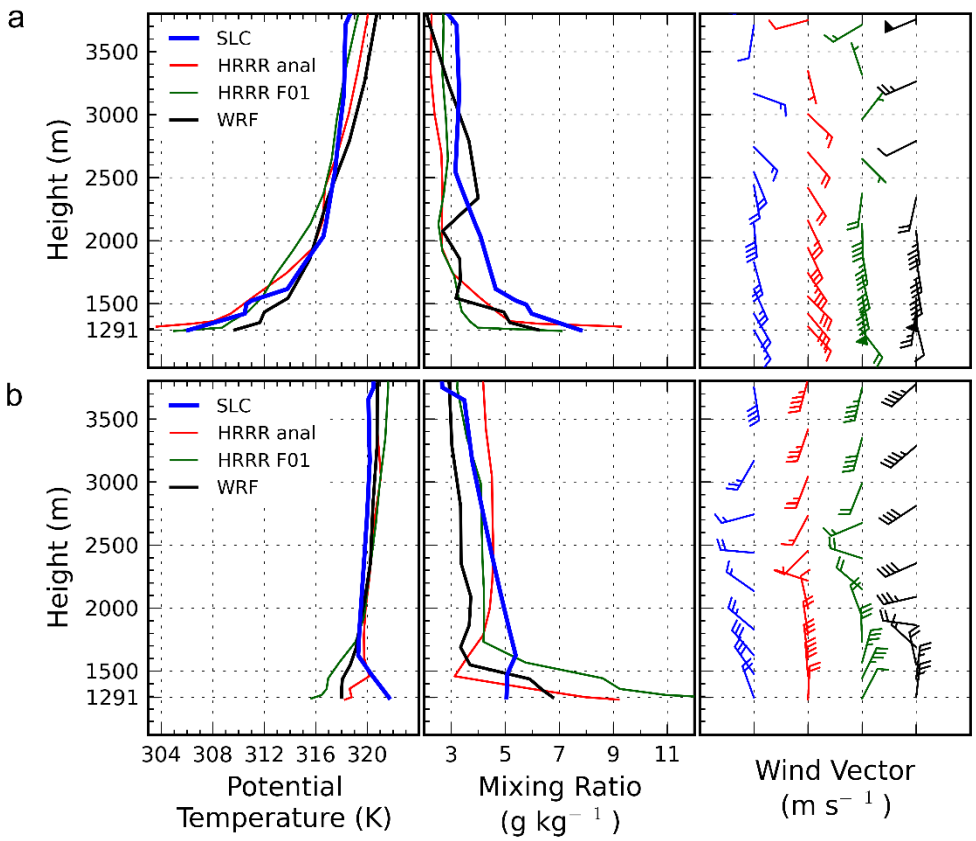

Figure 3.1. Vertical profiles of potential temperature, mixing ratio, and vector winds at SLC from the SLC rawinsonde (blue), HRRR analysis (red), HRRR 1-h forecast (green) and WRF simulation (black) at: (a) 1200 UTC 18 June 2015 and (b) 0000 UTC 19 June 2015. Half, full, and flag wind barb denotes 1, 2, and 10 m s^{-1}, respectively.

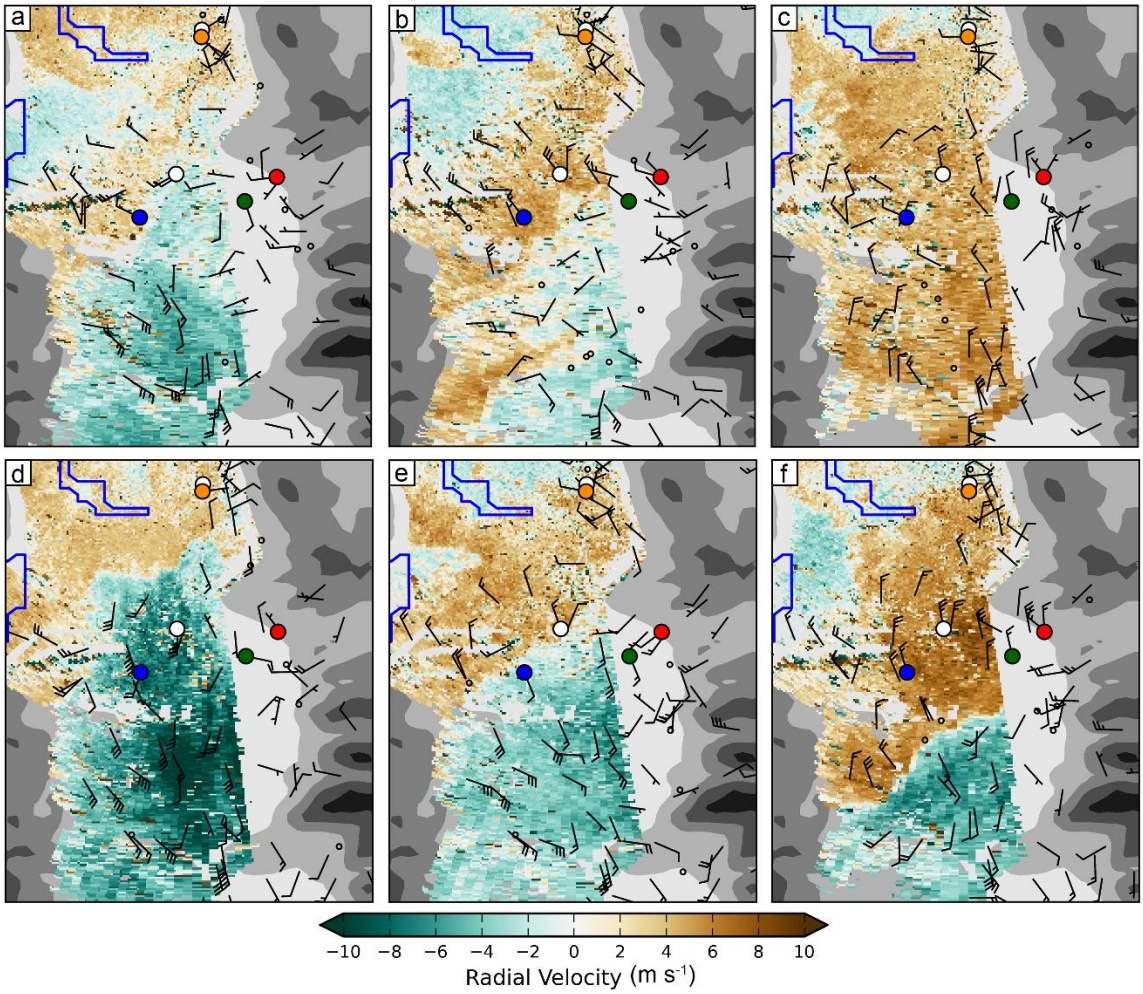

Figure 3.2. TDWR 0.5° radial velocity and MesoWest surface wind observations. 17 June 2015: (a) 1800, (b) 2100 UTC, and (c) 0000 UTC. 18 June 2015: (d) 1800 (e) 2100 UTC and (f) 0000 UTC. Terrain is indicated by successively darker grey shades at 500 m intervals with the approximate shoreline of the Great Salt Lake outlined in blue. Color shading indicates radial velocity with respect to the TDWR located at the top of the map, according to the color bar. Vector winds at observation sites marked by wind barbs where a half and full barb denotes 1 and 2 m s-1, respectively. Colored dots denote observation sites highlighted in Figure 1.3b.

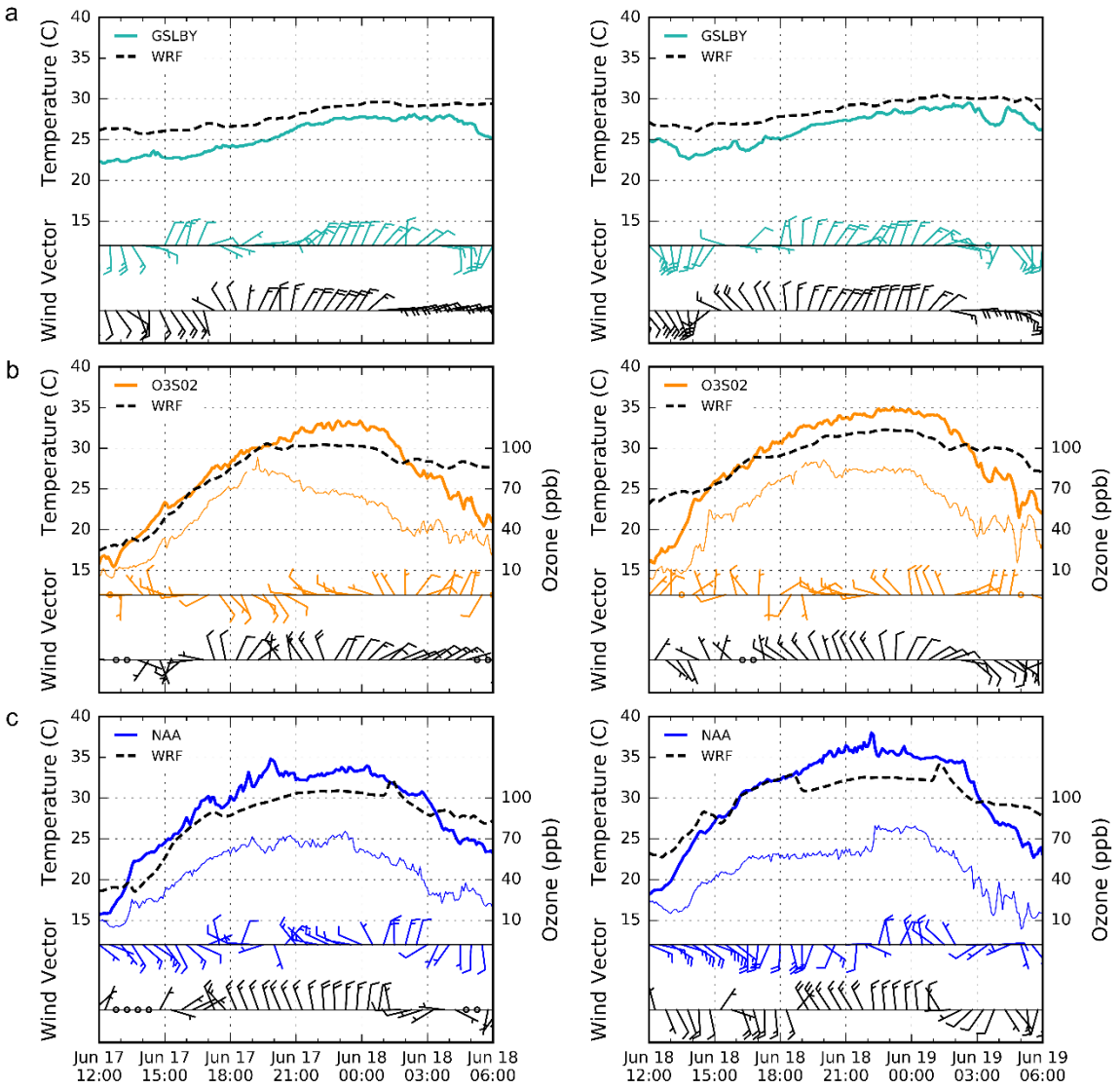

Figure 3.3. Observed (thick color) and simulated (dashed black) temperature, observed ozone (thin color) and vector wind between 1200 UTC 17 June 2015 and 0600 UTC 18 June 2015 (left) and 1200 UTC 18 June 2015 and 0600 UTC 19 June 2015 (right). Wind barbs are plotted every half hour with half and full barbs denoting 1 and 2 m s-1, respectively.

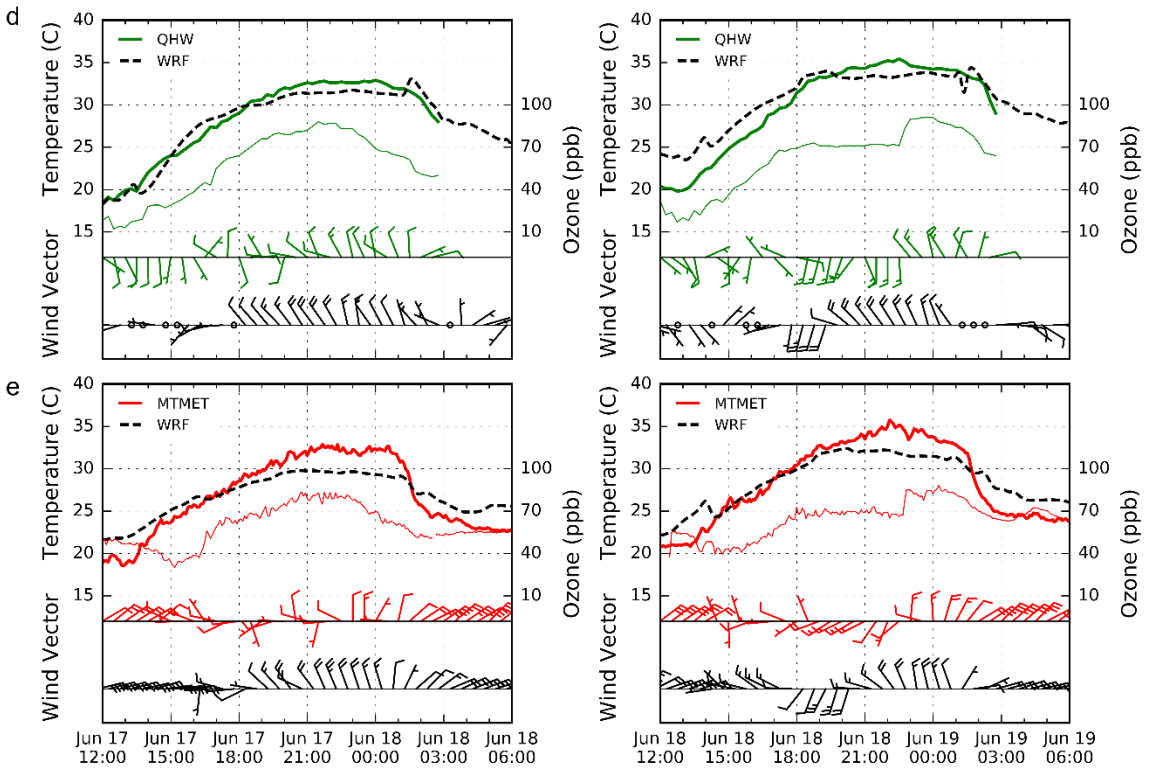

Figure 3.3. Continued

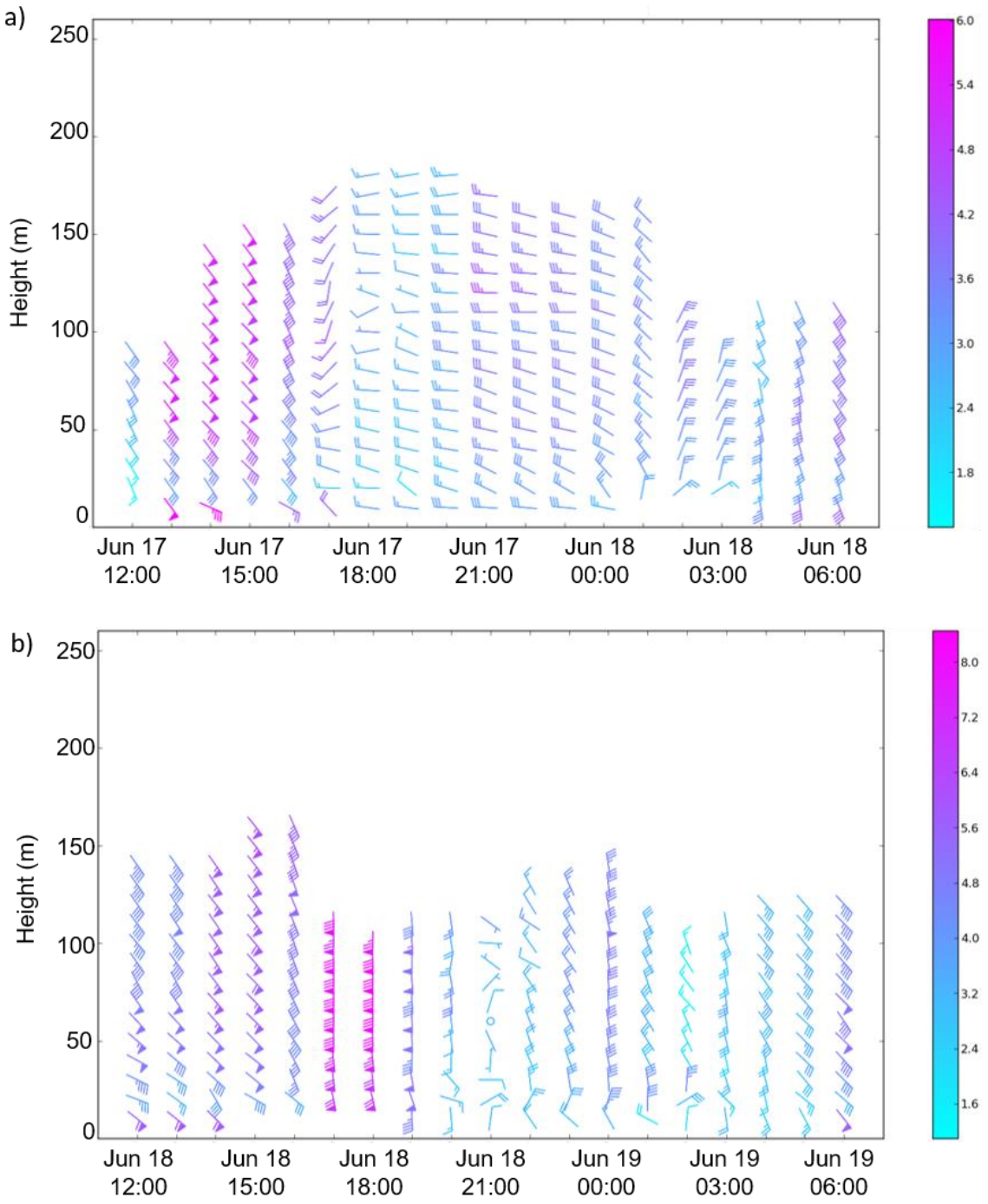

Figure 3.4. Vector winds measured by sodar approximately 5 km north of NAA between 1200 and 0600 UTC on a) 17 June 2015 and b) 18 June 2015. Half barb, full barb, and flag represent 0.5, 1, and 5 m s^{-1}, respectively. Wind speed also according to scale.

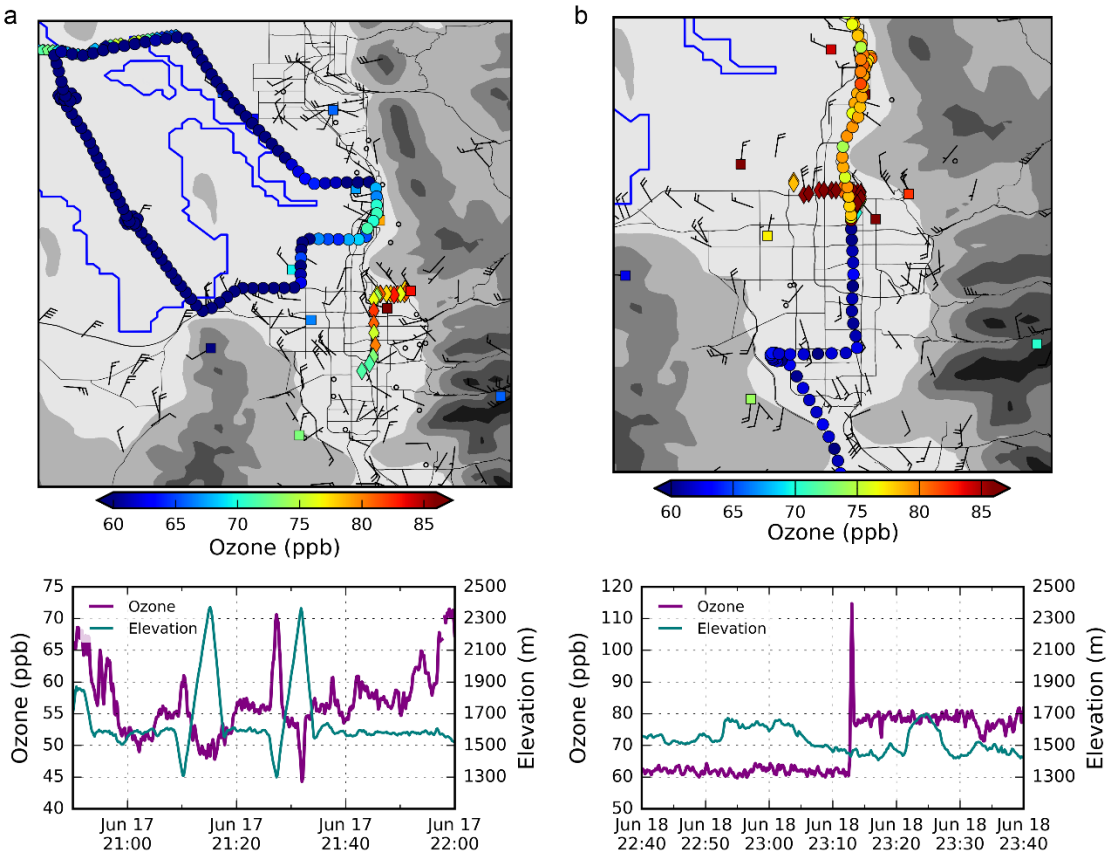

Figure 3.5. Ozone observations according to color bar (top) between (a) 2050-2200 UTC 17 June 2015 and (b) 2240-2340 UTC 18 June 2015. Mobile ozone observations from KSL helicopter (circles) and TRAX (diamonds) plotted every 30 s and 3 mins, respectively. Station sites show the most recent ozone (squares) and vector winds (barbs) observation within the hour ending at 2340 UTC. Major roads drawn in black with terrain shaded grey and lake outlined in blue. Time series (bottom) of ozone concentration (purple) and elevation (teal) during the helicopter flights. As a reference, surface elevation ~1300 m.

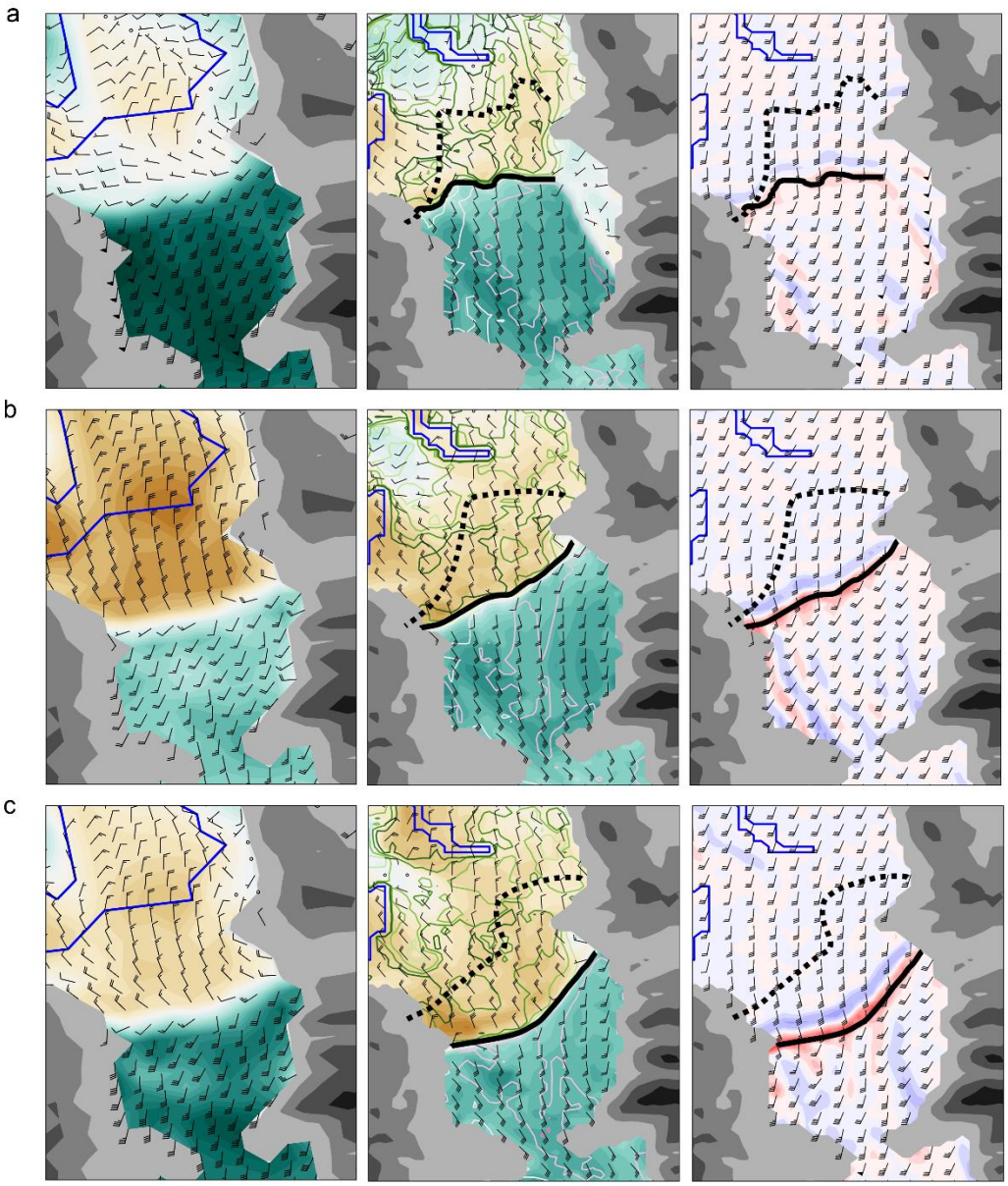

Figure 3.6. Simulated wind and moisture fields on 18 June 2015 at (a) 1800, (b) 1900, (c) 2000 (d) 2100 (e) 2200, and (f) 2300 UTC. Lake boundary in HRRR and WRF outlined by blue line. For reference, the dashed and solid lines represent the progression of the observed and simulated lake-breeze front, respectively. Left panels: HRRR analysis 10-m meridional wind (shading) and 10-m vector winds (barbs). Middle panels: WRF 10-m meridional wind (shading), 10-m vector winds (barbs) and 2-m water vapor mixing ratio (contours). Right panels: WRF model level 7 (~1000 m AGL) vertical velocity (shading) and vector winds (barbs). Barbs are plotted every 3 km where half, full, and flag barbs denote 1, 2, and 10 m s-1, respectively.

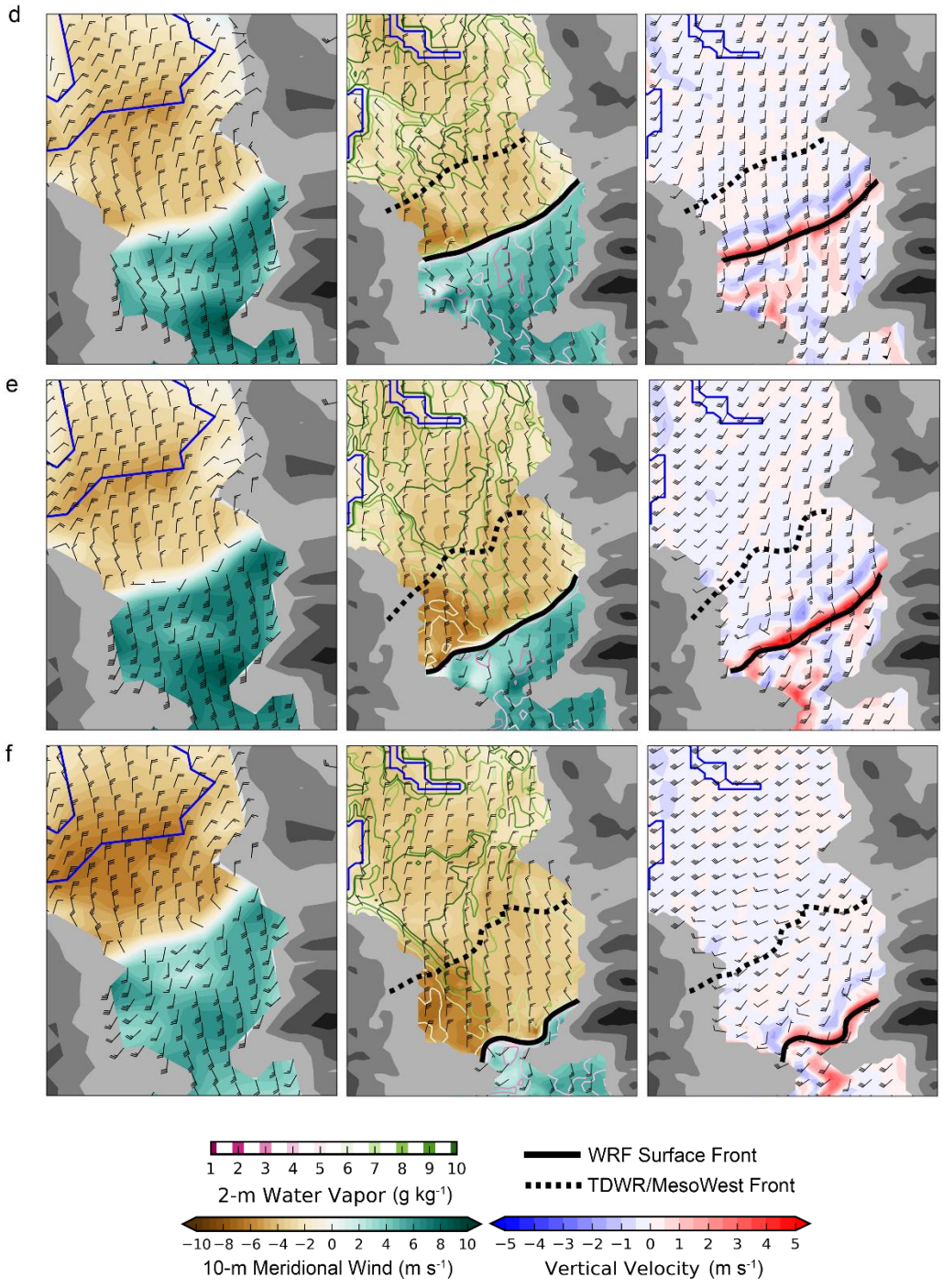

Figure 3.6. Continued

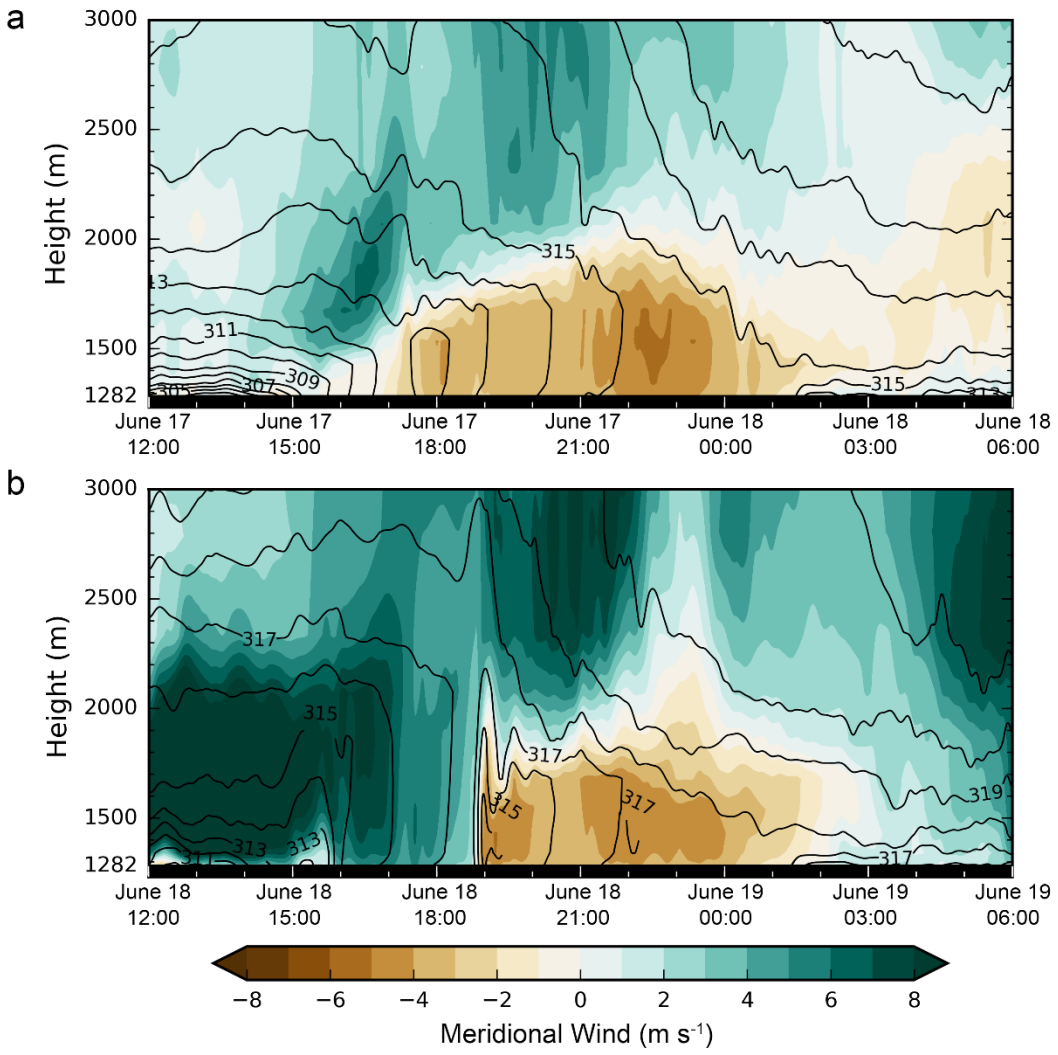

Figure 3.7. Time-height section of simulated meridional wind (shading) and potential temperature (contours at 1 K intervals) at NAA from (a) 1200 UTC 17 June 2015 to 0600 UTC 18 June 2015 and (b) 1200 UTC 18 June 2015 to 0600 UTC 19 June 2015.

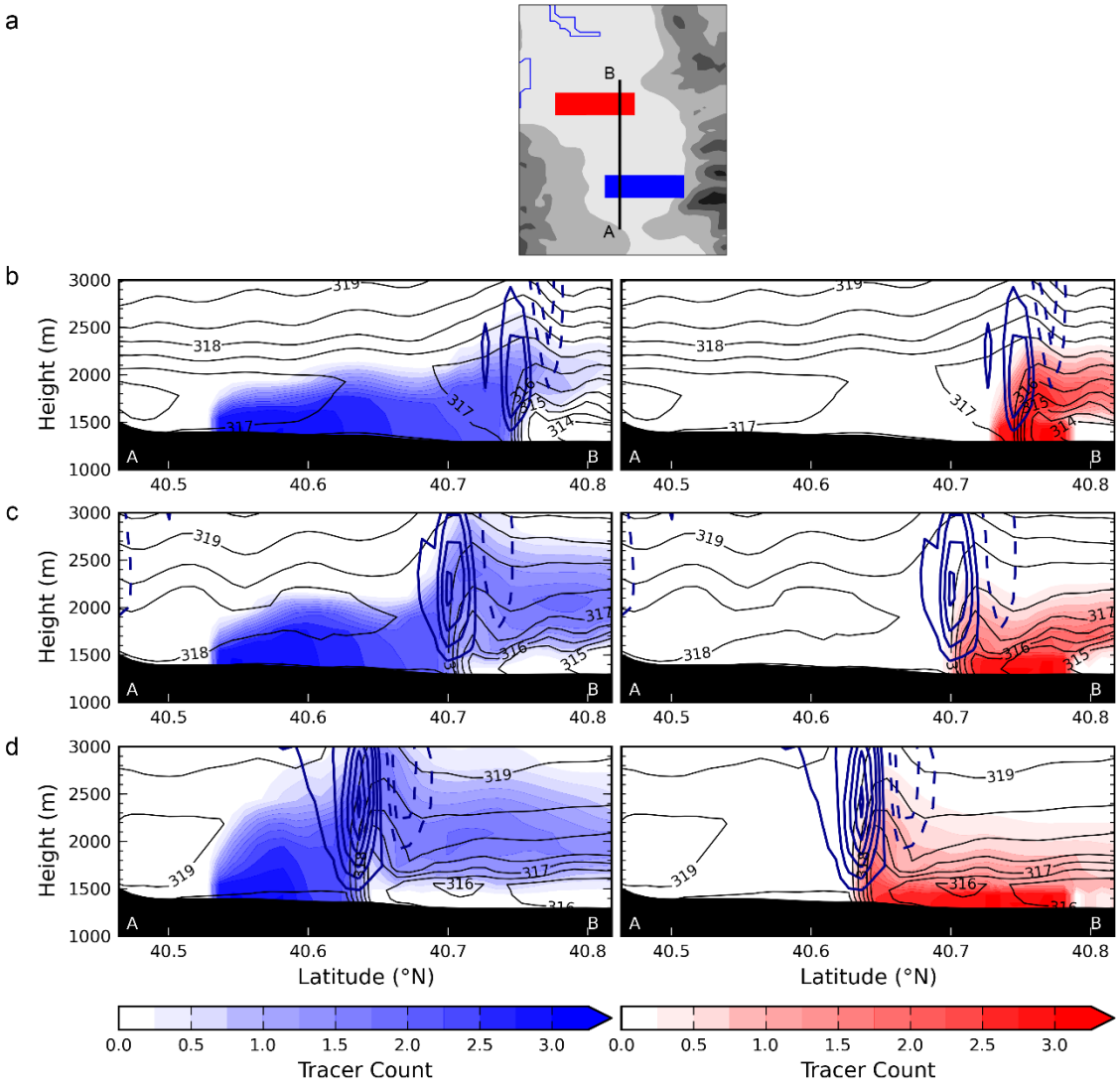

Figure 3.8. Vertical cross section of passive tracers and potential temperature. (a) Cross section orientation through the Salt Lake Valley from A to B and locations of source regions of southern (blue) and northern (red) tracers. Potential temperature (black contours at 0.5 K interval), upward (blue solid) and downward (blue dashed) vertical velocity contoured at 0.5 m s-1, and passive tracer concentrations on 18 June 2015 at: (b) 1800 UTC (c) 1900 UTC (d) 2000 UTC. Left and right panels denote the transport of the southern and northern tracers, respectively.

CHAPTER 4

CONCLUSION

4.1 Summary

The impact of lake breezes on summer ozone concentrations in the Salt Lake Valley was investigated using data from $GSLSO_3S$ conducted during summer 2015. Knowledge of the areal extent of ozone over and surrounding the GSL preceding and during the high-ozone event on 18 June 2015 was made possible by the extensive meteorological and ozone observation network available during $GSLSO_3S$ (Horel et al. 2016), and a numerical weather simulation of the event demonstrates how pollution is transported by the lake breeze.

Over the course of a few days in mid-June, ozone built up in the vicinity of the GSL to unhealthy levels. On 17 June, ozone within the urban area of the Salt Lake Valley was higher than concentrations measured over the lake except for elevated ozone concentrations within the shallow, stable layer directly over the lake. On the following day, 18 June, the high ozone concentrations in the valley were only observed after the passage of the lake breeze. Observations from surface ozone monitors and a news helicopter showed that ozone concentrations within the lake breeze on 18 June were ~20 ppb higher than those over the urban areas farther south. The highest ozone concentrations preceding the lake breeze were observed at O3S02, which is situated near the marshy areas of the lake, where

natural and urban ozone precursors pool at night and are likely confined in a shallow boundary layer. After sunrise, these conditions likely contribute to rapid ozone formation. The ozone is then transported toward the urban areas by the lake breeze in the afternoon. The deeper boundary layer in the valley in which ozone and precursors are mixed through a larger depth is then replaced by the shallower lake-breeze boundary layer containing high ozone concentrations.

The characteristics of the lake breeze on 17 June conformed to typical lake breezes previously studied in the Salt Lake Valley, including distinct pulses up the valley in the afternoon until the northerly lake-breeze flow filled the entire valley by 0000 UTC. Ozone concentrations within the Salt Lake Valley were reduced by the advection of lower ozone air by the lake breeze. However, strong flow opposing the lake breeze on 18 June contributed to strong convergent frontogenesis. The opposing southerly winds kept the lake breeze at bay until 2100 UTC, when a single pulse pushed south through the Salt Lake Valley, several hours later than that observed the previous day. The lake-breeze front caused a sharp ~20 ppb increase in ozone at surface stations as well as aloft between 1400 and 1700 m ASL (100-300 m AGL). This increase in ozone within the lake breeze is similar to those observed by Wentworth et al. (2015), and elevated ozone levels persisted throughout the afternoon. The rapid increase and decrease in ozone observed aloft by the helicopter within the lake-breeze head is unique and is likely caused by the convergence of pollutants within the lake-breeze head and reduced titration there.

While the 3-km-resolution HRRR helps to resolve many complex thermal and terrain flows in northern Utah, subtle meteorological features such as the intensity of the southerly flow during late morning on 18 June were not captured by the HRRR analyses.

Overly intense lake breezes predicted by the HRRR may result in part from imperfect specification of the areal extent and temperature of the GSL. However, our research simulations of the two-day period, utilizing corrections to the lake size and temperature, did not deepen the lake boundary layer and weaken the simulated lake breeze as much as we were expecting. Hence, initializing the simulation even earlier than we have done here may be necessary to allow the model's lake boundary layer to adjust to the modified surface state.

While far from perfect, the simulation at 1-km resolution captured many of the features of the weaker lake breeze on 17 June and the stronger lake breeze on 18 June. However, the simulation missed a very subtle, short-lived strengthening of the southerly opposing flow on 18 June, which affected the timing of the simulated lake-breeze propagation, whereas the observed lake breeze propagation was delayed. Still, the simulation is useful in understanding the dynamics of pollution transport and dispersion by a strong lake-breeze font. Passive tracers released within the model simulation on 18 June highlight the distinct transports ahead of and behind the lake-breeze front.

The findings presented in this work should be useful to local air quality forecasters as well as forecasters and modelers in other coastal regions where frequent lake- or sea-breeze circulations impact pollution levels. This study highlights how the timing and intensity of subtle mesoscale features, such as the short burst of southerly flow observed midday on 18 June, can affect a lake breeze and ozone concentrations within an urban region later in the afternoon. Air quality forecasters and researchers should be aware of these model limitations and make adjustments when necessary. This work also demonstrates how real-time observations may be useful to forecasters and research who

evaluate local pollution events as they occur.

4.1 Future Work

Modifications to the lake size and temperature in the numerical weather model presented in this thesis were "low-hanging fruit" improvements made to our research simulation. Because of the impact lake size and temperature have on simulated lake breezes, improved and updated lake masks and land surface characteristics should be implemented in operational weather models and updated regularly. In addition, improved geographical data sets should be made available to the research community at high resolutions for use in high resolution research simulations. Aside from improved surface states, planetary boundary layer schemes used for lake-breeze simulations should also be investigated, which has not been explored as part of this study.

The need for updated land characteristics has been recognized by the National Oceanic and Atmospheric Administration's (NOAA) Earth System Research Laboratory. According to Trevor Alcott (email communication), an updated land surface geographical data set with additional modifications to the GSL lake mask is being implemented in the experimental version of the HRRR model. The impact of this change should be investigated and later implemented into the operational HRRR at NCEP.

The modification discussed in section 2.2.2 describes how lake temperature was crudely reinitialized as a uniform value based on available observations for the duration of the model simulation. This method does not account for the spatial and temporal variations in the lake's water temperature. The reason for this simplified approach is due to limitations of the WRF model, which is unable to simulate time-varying lake surface temperatures.

Therefore, improved surface temperature estimates used for model initialization as well as development of time-varying lake surface temperature simulations through the use of a lake-atmosphere-coupled model would be beneficial to lake breeze and coastal environment forecasting. In respect to initialized lake temperature, according to communication between a colleague and Rob Grumbine at NOAA, the HRRR currently initializes the lake surface temperature with the low-resolution Real-time Global (RTG) product, whereas other operational models, such as the North America Mesoscale model and Global Forecast System, use high-resolution RTG products. Use of the high-resolution RTP products in the HRRR model should also be investigated. Improvements to the HRRR's lake area and temperature would not only benefit lake-breeze forecasts, but also improve forecasts of convection near the lake and lake-effect snow, which are weather events also dependent on the lake's size and temperature.

Rather than making case-by-case custom modifications for small domains, as has been performed in this study, a better approach to improving the surface state of simulations would be to take advantage of remote sensing products such as the Moderate Resolution Imaging Spectroradiometer (MODIS) and Visible Infrared Imaging Radiometer Suite (VIIRS) satellite sensors. For example, improved use of remotely sensed water surface temperatures can better estimate coastal and lake surface temperatures and capture the spatial and temporal variability in water temperature. It is expected that adjusting sea and lake temperatures closer to observations and initializing the model earlier to allow additional time for the boundary layer to adjust to the surface conditions would improve the model's treatment of the stable boundary layer over oceans and lakes as well as the onset of the sea and lake breeze penetrating the urban area.

The UCACN Model Advisory Committee recognizes the need for a land data assimilation system (LDAS) that weather models could use to initialize surface parameters (Report of the UCACN Model Advisory Committee 2015). In current state-of-the-art weather models, like the WRF model, some surface fields, such as green vegetation fraction and albedo, rely on climatology rather than real-time or recent observations. The initial surface characteristics in the WRF model can be improved by ingesting available satellite observations, including sea surface temperature, skin temperature, green vegetation fraction, urban properties, and soil moisture. Previous studies have shown that using this type of data greatly benefits WRF model performance (Case et al. 2011; Kumar et al. 2014). NASA's Short-term Prediction Research and Transition Center (SPoRT) provides MODIS products that can be used to improve WRF simulations. SPoRT products have typically been used to improve modeled convection, heavy precipitation, drought monitoring, as well as other applications. Future research will expand SPoRT applications to improve understanding and forecastability of thermally driven flows and air quality in urban cities near coastal environments.

Future work will investigate available products and resources that can be ingested in the WRF model, and the sensitivity of those products will be evaluated with the focus of improving model performance in urban-coastal environments. The use of VIIRS data in WRF simulations is especially worth investigating because VIIRS is a newer instrument that builds on the capabilities of MODIS and AVHRR instruments. These improvements may produce better simulations of wind fields around lakes and oceans, which influence the dispersion and transport of ozone precursors. While the work presented in this thesis focuses on the Great Salt Lake, other coastal areas will likely benefit from surface state

improvements when applied on a continental scale.

Another source of model error may be introduced by the planetary boundary layer schemes used in this study. The simulation shown in this thesis used the Mellor-Yamada-Janijic scheme (Table 2.1), but a different scheme or modified mixing parameters may be more appropriate for the Great Salt Lake area. Prior work done in the Galveston Bay area in Texas found that the Mellor-Yamada-Janijic scheme had larger temperature, moisture, and boundary layer height biases than other schemes used in the WRF model (Hu et al. 2010). Similar differences between boundary layer schemes in the Great Salt Lake area may be found, but additional work is required to find the best options for lake-breeze events.

This work can be accomplished first by continued focus on improving surface state in WRF simulations around the Great Salt Lake and testing different boundary layer schemes. The reason for this continued focus is that there is a large set of data available from GSLSO_3S. From that field study there is a wealth of meteorological and ozone data that can be used to verify the model simulations. Observations in the Salt Lake Valley will continue in upcoming summers, though not as extensive as was performed in 2015. The end goal is to use these observations to evaluate the use of remote sensed products in the WRF model for the GSL area and other coastal areas of interest. Improvements to simulated winds and boundary layer structure in coastal environments will in turn benefit air quality simulations.

After the use of additional remote sensing products and appropriate boundary layer schemes in the WRF model are rigorously tested, those improvements should be implemented in the WRF-Chem model. It is expected that improvements to the wind field

and boundary layer structure will improve modeled ozone formation, its recirculation, and dispersion. While the passive tracers are useful for understanding pollution transport by a lake-breeze front, a full chemistry model has not been used in this study. To more completely understand ozone pollution in coastal regions, a chemistry model would need to be used since the passive tracers do not experience chemical reactions.

While improved land surface initialization is one necessary step to improve numerical models of weather and air chemistry, the predictability of some events will still be limited. As shown for the 18 June 2015 lake breeze, subtle atmospheric influences on scales unresolved by operational mesoscale models may impede the predictability of localized pollution events. Improvements in predictability of these small-scale features will likely come from better numerical physics and parameterizations, boundary conditions, and computing resources.

In summary, high-resolution simulations of thermally driven flows near coastal environments important to air quality forecasts could be improved if they are initialized with improved surface conditions. These modifications are important because boundary layer processes are sensitive to surface characteristics. Timely completion of this work would advance the knowledge and predictability of poor air quality events near the GSL and other coastal environments. Finally, HRRR-initialized WRF simulations may benefit other aspects of numerical modeling research, especially as HRRR model updates come online. At the time of this publication there is no official HRRR analyses archive.

REFERENCES

Angevine, W. M., M. Tjernström, and M. Žagar, 2006: Modeling of the coastal boundary layer and pollutant transport in New England. *J. Appl. Meteor. Climatol.* 45, 137–154, doi:10.1175/JAM2333.1.

Angevine, W. M., L. Eddington, K. Durkee, C. Fairall, L. Bianco, and J. Brioude, 2012: Meteorological model evaluation for CalNex 2010. *Mon. Wea. Rev.* 140, 3885–3906, doi:10.1175/MWR-D-12-00042.1.

Arritt, R. W. 1989: Numerical modelling of the offshore extent of sea breezes. *Quart. J. Roy. Meteor. Soc.* 115, 547–570, doi:10.1002/qj.49711548707.

Arritt, R. W. 1993: Effects of the large-scale flow on characteristic features of the sea breeze. *J. Appl. Meteor. Climatol.* 32, 116–125, doi:10.1175/1520-0450(1993)032<0116:EOTLSF>2.0.CO;2.

Banta, R. M., and Coauthors, 2005: A bad air day in Houston. *Bull. Amer. Meteor. Soc.* 86, 657–669, doi:10.1175/BAMS-86-5-657.

Bao, J-W., S. A. Michelson, P. O. G. Persson, I. V. Djalalova, and J. M. Wilczak, 2008: Observed and WRF-simulated low-level winds in a high-ozone episode during the Central California Ozone Study. *J. Appl. Meteor. Climatol.* 47, 2372–2394, doi:10.1175/2008JAMC1822.1.

Benjamin, S. G., and Coauthors, 2016: A North American hourly assimilation and model forecast cycle: The Rapid Refresh. *Mon. Wea. Rev.* 144, 1669-1694, doi:10.1175/MWR-D-15-0242.1.

Blaylock, B. K., J. D. Horel, and E. T. Crosman, 2016: Impact of a lake breeze on summer ozone concentration in the Salt Lake Valley. *J. Appl. Meteor. Climatol.* Submitted.

Burley, J. D., S. Theiss, A. Bytnerowicz, A. Gertler, S. Schilling, and B. Zielinska, 2015: Surface ozone in the Lake Tahoe Basin. *Atmos. Environ.* 109, 351–369, doi:10.1016/j.atmosenv.2015.02.001.

Case, J. L., S. V. Kumar, J. Srikishen, and G. J. Jedlovec, 2011: Improving numerical weather predictions of summertime precipitation over the Southeastern United

States through a high-resolution initialization of the surface state. *Wea. Forecasting* 26, 785–807. doi: 10.1175/2011WAF2222455.1.

Crosman, E., and J. Horel, 2009: MODIS-derived surface temperature of the Great Salt Lake. *Remote Sensing of Environment.* 113, 73-81, doi:10.1016/j.rse.2008.08.013.

Crosman, E., and J. Horel, 2010: Sea and lake breezes: A review of numerical studies. *Boundary-Layer Meteor.* 137, 1-29, doi:10.1007/s10546-010-9517-9.

Crosman, E., and J. Horel, 2012: Idealized large-eddy simulations of sea and lake breezes: sensitivity to lake diameter, heat flux and stability. *Boundary-Layer Meteor.* 144, 309-328, doi:10.1007/s10546-012-9721-x.

Crosman, E., and J. Horel, 2016: Winter lake breezes near the Great Salt Lake. *Boundary Layer Meteor.* 159, 439–464, doi:10.1007/s10546-015-0117-6.

Environmental Protection Agency, 2015: Implementation of the 2015 primary ozone NAAQS: Issues associated with background ozone. *White Paper for Discussion.* Accessed 6 June 2016. [Available online at http://www3.epa.gov/airquality/ozonepollution/pdfs/whitepaper-bgo3-final.pdf.]

Foley, T., E. A. Betterton, P. E. Robert Jacko, and J. Hillery, 2011: Lake Michigan air quality: The 1994–2003 LADCO Aircraft Project (LAP). *Atmos. Environ.* 45, 3192-3202, doi:10.1016/j.atmosenv.2011.02.033.

Gaza, R., 1998: Mesoscale meteorology and high ozone in the Northeast United States. *J. Appl. Meteor. Climatol.* 37, 961-977, doi:10.1175/1520-0450(1998)037<0961:MMAHOI>2.0.CO;2.

Gilliam, R. C., S. Raman, and D. D. S. Niyogi, 2004: Observational and numerical study on the influence of large-scale flow direction and coastline shape on sea-breeze evolution. *Boundary-Layer Meteor.* 111, 275–300, doi:10.1023/B:BOUN.0000016494.99539.5a.

Hastie, D. R., and Coauthors, 1999: Observational evidence for the impact of the lake breeze circulation on ozone concentrations in southern Ontario. *Atmos. Environ.* 33, 323-335, doi:10.1016/S1352-2310(98)00199-X.

Hayden, K. L., and Coauthors, 2011: Aircraft study of the impact of lake-breeze circulations on trace gases and particles during BAQS-Met 2007. *Atmos. Chem. Phys.* 11, 10173-10192, doi:10.5194/acp-11-10173-2011.

Horel, J., and Coauthors, 2002: Mesowest: Cooperative mesonets in the Western United States. *Bull. Amer. Meteor. Soc.* 83, 211–225, doi:10.1175/1520-0477(2002)083<0211:MCMITW>2.3.CO;2.

Horel, J., E. Crosman, A. Jacques, B. Blaylock, S. Arens, A. Long, J. Sohl, and R. Martin, 2016: Influence of the Great Salt Lake on summer air quality over nearby urban areas. *Atmospheric Science Letters.* Accepted.

Hu, X.-M., J. W. Neilson-Gammon, F. Zhang, 2010: Evaluation of three planetary boundary layer schemes in the WRF model. *J. Appl. Meteor. Climatol.* 49, 1831-1844. doi: 10.1175/2010JAMC2432.1.

Hwang, M-K., Y-K. Kim, S. N. Oh, H. W. Lee, and C-H. Kim, 2007: Identification and interpretation of representative ozone distributions in association with the sea breeze from different synoptic winds over the coastal urban area in Korea. *J. Air Waste Manage.* Assoc. 57, 1480-1488, doi:10.3155/1047-3289.57.12.1480.

Jaffe, D., 2011: Relationship between surface and free tropospheric ozone in the Western U.S. *Environ. Sci. Technol.* 45, 432-438, doi:10.1021/es1028102.

Ji, H-E., S-H. Lee, and H-W. Lee, 2013: Characteristics of sea breeze front development with various synoptic conditions and its impact on lower troposphere ozone formation. *Adv. Atmos. Sci.* 30, 1461-1478, doi:10.1007/s00376-013-2256-3.

Kumar, A., F. Chen, M. Barlage, M. B. Ek, and D. Niyogi, 2014: Assessing Impacts of integrating MODIS vegetation data in the Weather Research and Forecasting (WRF) model coupled to two different canopy-resistance approaches. *J. Appl. Meteor. Climatol.* 53, 1362–1380. doi: 10.1175/JAMC-D-13-0247.1.

Lareau, N. P., and J. Horel, 2015: Dynamically induced displacements of a persistent cold-air pool. *Boundary-Layer Meteor.* 154, 291-316, doi:10.1007/s10546-014-9968-5.

Lennartson, G. J., and M. D. Schwartz, 2002: The lake breeze-ground level ozone connection in eastern Wisconsin: A climatological perspective. *Int. J. Climatol.* 22, 1347-1364, doi:10.1002/joc.802.

Levy, I., and Coauthors, 2010: Unraveling the complex local-scale flows influencing ozone patters in the southern Great Lakes of North America. *Atmos. Chem. Phys.* 10, 10895-10915, doi:10.5194/acp-10-10895-2010.

Lombardo, K., E. Sinsky, Y. Jia, M. M. Whitney, and J. Edson, 2016: Sensitivity of simulated sea breezes to initial conditions in complex coastal regions. *Mon. Wea. Rev.* 144, 1299-1320, doi:10.1175/MWR-D-15-0306.1.

Lu, R., and R. P. Turco, 1995: Air pollutant transport in a coastal environment—II. Three-dimensional simulations over Los Angeles basin. *Atmos. Environ.* 29, 1499-1518, doi:10.1016/1352-2310(95)00015-Q.

Ludwig, F. L., J. Horel, and C. D. Whiteman, 2004: Using EOF analysis to identify

important surface wind patterns in mountain valleys. *J. Appl. Meteor.* Soc. 43, 969-983, doi:10.1175/1520-0450(2004)043<0969:UEATII>2.0.CO;2.

Miller, S. T. K., B. D. Keim, R. W. Talbot, and H. Mao, 2003: Sea breeze: structure, forecasting, and impacts. *Rev. Geophys.* 41, 1-31. doi: 10.1029/2003RG000124.

Oh, I-B., Y-K. Kim, H. W. Lee, and C-H. Kim, 2006: An observational and numerical study on the effects of the late sea breeze on ozone distributions in the Busan metropolitan area, Korea. *Atmos. Environ.* 40, 1284-1298, doi:10.1016/j.atmosenv.2005.10.049.

Porson, A., D. G. Steyn, and G. Schayes, 2007: Sea breeze scaling from numerical model simulations, part II: Interactions between the sea breeze and slope flows. *Boundary-Layer Meteor.* 122, 31–41, doi:10.1007/s10546-006-9092-2.

Report of the UCACN model advisory committee. 2015: *UMAC Final Report* [Available online at: http://www.ncep.noaa.gov/director/ucar_reports/ ucacn_20151207/UMAC_Final_Report_20151207-v14.pdf]

Sills, D. M. L., J. R. Brook, I. Levy, P. A. Makar, J. Zhang, and P. A. Taylor. 2011: Lake breezes in the southern Great Lakes region and their influence during BAQS-Met 2007. *Atmos. Chem. Phys.* 11, 7955-7973, doi:10.5194/acp-11-7955-2011.

Sousa, S. I. V., M. C. M. Alvim-Ferraz, and F. G. Marins, 2013: Health effects of ozone focusing on childhood asthma: What is now known—a review from an epidemiological point of view. *Chemosphere*. 90, 2051-2058, doi:10.1016/j.chemosphere.2012.10.063.

Stauffer, R. M., and Coauthors, 2015: Bay breeze influence on surface ozone at Edgewood, MD during July 2011. *J. Atmos. Chem.* 69, 335-353, doi:10.1007/s10874-012-9241-6.

Stewart, J. Q., C. D. Whiteman, W. J. Steenburgh, and X. Bian, 2002: A climatological study of thermally driven wind systems of the U.S. Intermountain West. *Bull. Amer. Meteor. Soc.* 83, 699-708, doi:10.1175/1520-0477(2002)083<0699:ACSOTD>2.3.CO;2.

Wentworth, G. R., J. G. Murphy, and D. M. L. Sills, 2015: Impact of lake breezes on ozone and nitrogen oxides in the Greater Toronto Area. *Atmos. Environ.* 109, 52-60, doi:10.1016/j.atmosenv.2015.03.002.

Wurtsbaugh, W., C. Miller, S. Null, P. Wilcock, M. Hahnenberger, and F. Howe, 2016: Impacts of water development on Great Salt Lake and the Wasatch Front. *Watershed Sciences Faculty Publications.* Paper 875. Accessed 6 June 2016. [Available online at http://digitalcommons.usu.edu/wats_facpub/875.]

Zumpfe D. E., and J. Horel, 2007: Lake-breeze fronts in the Salt Lake Valley. *J Appl. Meteor. Climatol.* 46, 196-211, doi:10.1175/JAM2449.1.